



This is a repository copy of *Peeling back the layers of crassulacean acid metabolism: functional differentiation between Kalanchoë fedtschenkoi epidermis and mesophyll proteomes*.

White Rose Research Online URL for this paper:
<https://eprints.whiterose.ac.uk/160900/>

Version: Published Version

Article:

Abraham, P.E., Hurtado Castano, N., Cowan-Turner, D. et al. (6 more authors) (2020) Peeling back the layers of crassulacean acid metabolism: functional differentiation between Kalanchoë fedtschenkoi epidermis and mesophyll proteomes. *The Plant Journal*, 103 (2). pp. 869-888. ISSN 0960-7412

<https://doi.org/10.1111/tpj.14757>

Reuse

This article is distributed under the terms of the Creative Commons Attribution (CC BY) licence. This licence allows you to distribute, remix, tweak, and build upon the work, even commercially, as long as you credit the authors for the original work. More information and the full terms of the licence here:
<https://creativecommons.org/licenses/>

Takedown

If you consider content in White Rose Research Online to be in breach of UK law, please notify us by emailing eprints@whiterose.ac.uk including the URL of the record and the reason for the withdrawal request.



eprints@whiterose.ac.uk
<https://eprints.whiterose.ac.uk/>

RESOURCE

Peeling back the layers of crassulacean acid metabolism: functional differentiation between *Kalanchoë fedtschenkoi* epidermis and mesophyll proteomes

Paul E. Abraham¹, Natalia Hurtado Castano^{2,3}, Daniel Cowan-Turner², Jeremy Barnes², Suresh Poudel^{1,4}, Robert Hettich¹, Sabrina Flütsch⁵, Diana Santelia⁵ and Anne M. Borland^{2,6*} 

¹Chemical Sciences Division, Oak Ridge National Laboratory, Oak Ridge, TN 37831, USA,

²School of Natural and Environmental Sciences, Newcastle University, Newcastle upon Tyne NE1 7RU, UK,

³Department of Molecular Biology and Biotechnology, University of Sheffield, Sheffield S10 2TN, UK,

⁴Department of Genome Science and Technology, University of Tennessee, Knoxville, TN 37996, USA,

⁵Institute of Integrative Biology, ETH, Zürich, Switzerland, and

⁶Biosciences Division, Oak Ridge National Laboratory, Oak Ridge, TN 37831, USA

Received 21 November 2019; revised 18 March 2020; accepted 23 March 2020.

*For correspondence (e-mail anne.borland@newcastle.ac.uk).

SUMMARY

Crassulacean acid metabolism (CAM) is a specialized mode of photosynthesis that offers the potential to engineer improved water-use efficiency (WUE) and drought resilience in C₃ plants while sustaining productivity in the hotter and drier climates that are predicted for much of the world. CAM species show an inverted pattern of stomatal opening and closing across the diel cycle, which conserves water and provides a means of maintaining growth in hot, water-limited environments. Recent genome sequencing of the constitutive model CAM species *Kalanchoë fedtschenkoi* provides a platform for elucidating the ensemble of proteins that link photosynthetic metabolism with stomatal movement, and that protect CAM plants from harsh environmental conditions. We describe a large-scale proteomics analysis to characterize and compare proteins, as well as diel changes in their abundance in guard cell-enriched epidermis and mesophyll cells from leaves of *K. fedtschenkoi*. Proteins implicated in processes that encompass respiration, the transport of water and CO₂, stomatal regulation, and CAM biochemistry are highlighted and discussed. Diel rescheduling of guard cell starch turnover in *K. fedtschenkoi* compared with that observed in *Arabidopsis* is reported and tissue-specific localization in the epidermis and mesophyll of isozymes implicated in starch and malate turnover are discussed in line with the contrasting roles for these metabolites within the CAM mesophyll and stomatal complex. These data reveal the proteins and the biological processes enriched in each layer and provide key information for studies aiming to adapt plants to hot and dry environments by modifying leaf physiology for improved plant sustainability.

Keywords: crassulacean acid metabolism, proteomics, epidermis, guard cell, starch metabolism.

INTRODUCTION

The water-conserving features of crassulacean acid metabolism (CAM) have highlighted this specialized mode of photosynthesis as a model for engineering improved water-use efficiency and drought resilience into C₃ crops (Borland *et al.*, 2014; Yang *et al.*, 2015). CAM is a syndrome of anatomical, metabolic and physiological adaptations that facilitate CO₂ concentration around ribulose-1,5-

bisphosphate carboxylase/oxygenase (rubisco), while circumventing approximately 90% of the water loss associated with stomatal transpiration at little or no cost to photosynthetic carbon assimilation (Shameer *et al.*, 2018). CAM improves the water-use efficiency (WUE = CO₂ fixed per unit water lost) of plants by up to 10-fold, compared with other types of photosynthesis, by enabling CO₂ uptake through open stomata and through CO₂ storage as

malate at night, when transpiration is reduced (Borland *et al.*, 2009). The subsequent decarboxylation of malate during the day releases CO₂, which is re-fixed by rubisco behind closed stomata. CAM is present in over 400 distinct genera across 36 families of vascular plants that are found in diverse ecosystems, ranging from semi-arid deserts to seasonally dry forests (Yang *et al.*, 2015). The multiple, independent evolutionary origins of CAM indicate that this water-conserving mode of photosynthesis is built on sets of genes common to plants that use conventional C₃ photosynthesis. Thus, it has been argued that the synthetic engineering of CAM in C₃ plants as a means of improving plant WUE is feasible by a rewiring of the core genetic and physiological regulatory circuits (Borland *et al.*, 2014, 2015; DePaoli *et al.*, 2014). The recent sequencing of several CAM genomes that evolved CAM independently have paved the way for identifying prospective components for engineering CAM into a C₃ background (Yang *et al.*, 2015). In particular, the availability of the genome of the constitutive species *Kalanchoë fedtschenkoi* (Yang *et al.*, 2017) provides a platform for establishing the functional genomics of CAM in a model system with straightforward plant transformation procedures and a wealth of documented biochemistry and whole-plant physiology data (Dever *et al.*, 2015; Hartwell *et al.*, 2016; Boxall *et al.*, 2017, 2020). Insights acquired from systems analysis of *K. fedtschenkoi* are expected to highlight the molecular basis of key traits that could be engineered into non-CAM plants to sustainably enhance productivity and survival in a hotter, drier world.

Central to the water-conserving traits of CAM sits a diel cycle of stomatal movement that operates in reverse to that of plants with C₃ or C₄ photosynthesis. Temporal reprogramming of the expression of genes implicated in the regulation of stomatal movement has been reported for CAM species such as *Agave americana*, *K. fedtschenkoi* and *Kalanchoë laxiflora*, relative to C₃ Arabidopsis (Abraham *et al.*, 2016; Yang *et al.*, 2017; Boxall *et al.*, 2020). Further work is required to define the diel turnover of proteins implicated in stomatal movement, in order to determine their distribution between the leaf mesophyll cells and stomatal complex, and to understand how mesophyll metabolism interacts with stomatal regulation. Current dogma suggests that CAM stomata are regulated via diel changes in the internal partial pressure of CO₂ (pCi) that accompany the diel turnover of malate in the leaf mesophyll (Borland *et al.*, 2014; Males and Griffiths, 2017). In addition to its proposed role as a mesophyll-derived signal that controls stomatal aperture, malate also plays a key role within the guard cells of C₃ plants for osmoregulation and as a counter ion for K⁺ (Santelia and Lawson, 2016). The existence of C₄/CAM-like metabolism in the guard cells of C₃ plants is well reported across the literature and is linked to the turnover of malate, which is generally

accepted as the predominant anion during C₃ stomatal opening and closing (Ferne and Martinoia, 2009). The contrasting roles for malate metabolism within the CAM mesophyll and stomatal complex present the hypothesis of tissue-specific regulation of malate turnover in the mesophyll and epidermal layer, containing the guard and subsidiary cells. Many of the proteins required for CAM are encoded by multigene families (Yang *et al.*, 2015; Yang *et al.*, 2017). Thus, it is possible that different isoforms responsible for nocturnal carboxylation and daytime malate decarboxylation carry out specific roles within the mesophyll and epidermis, with malate metabolism in the epidermis having implications for stomatal regulation. A better understanding of how proteins implicated in the diel metabolism of malate, as well as that of other primary metabolites such as starch, are organized between the epidermis and leaf mesophyll cells of CAM plants will provide insight on how metabolism within these spatially separated tissues has diverged from that in C₃ plants.

In addition to distinctive metabolic and physiological features, CAM species typically possess anatomical traits such as thickened, succulent leaves or stems (Borland *et al.*, 2018). Succulence facilitates the vacuolar storage of malic acid as well as water (Balsamo and Uribe, 1988; Rodrigues *et al.*, 2013), and enhances CO₂ trapping during the daytime decarboxylation of CAM by reducing the intercellular air space of the leaf (Borland *et al.*, 2018). Such anatomical characteristics are likely to impose specialized roles for proteins implicated in the transport of CO₂ and water within the mesophyll and epidermis. Reduced water permeability of the leaf cuticle also appears to be a key trait shared by CAM species. In addition to curtailing water loss, the composition of epicuticular wax influences heat load and photoprotection of leaves via reflectance and light dispersion (Shepherd and Griffiths, 2006; Bernard and Joubes, 2013). The daytime closure of stomata typifying CAM implies that heat tolerance is a critical adaptive trait for CAM plants. A better understanding of cuticular wax biochemistry in CAM species offers further opportunities for engineering enhanced heat and dehydration tolerance in plants.

We sought to provide a detailed proteome resource that captures the underlying biological functions responsible for the water-conserving and heat tolerance traits that typify CAM using the model CAM species *K. fedtschenkoi*. We performed large-scale quantitative comparisons between the leaf mesophyll and the guard cell complex isolated in epidermal peels to reveal the protein functions that exist in the mesophyll and epidermal layers, and to establish the spatial separation of protein function that exists between the two layers. As the essence of CAM is founded on diel control of metabolism and stomatal conductance, we also compared the temporal dynamics of epidermal and mesophyll proteomes over the 24-h light/dark cycle to better

define the cellular behaviors underpinning CAM in these functionally distinct tissues. Distinct pathways related to stomatal regulation, CAM biochemistry and guard cell starch metabolism were of particular interest and are therefore highlighted and discussed in this study.

RESULTS AND DISCUSSION

Tissue sampling within the context of the CAM cycle

Crassulacean acid metabolism (CAM) plants exhibit a diel separation of two major metabolic phases. At night, stomatal opening permits the net uptake of CO₂ (in the form of HCO₃⁻) by phosphoenolpyruvate carboxylase (PEPC) and the subsequent conversion to and storage of malic acid in the vacuole. During the day, decarboxylation of malate releases CO₂ for refixation by C₃ photosynthesis, behind closed stomata. A typical CAM gas-exchange profile for mature leaves (leaf pair 6, LP6) of *K. fedtschenkoi* is shown in Figure 1(a) to provide physiological context for the proteomics data obtained by sampling mesophyll and epidermis tissues over the diel cycle at 4-h intervals, as indicated.

Cell types and distribution of chloroplasts and mitochondria in the epidermis

In *K. fedtschenkoi*, stomata are surrounded by three or four subsidiary cells (Figure 1c), as reported for other species of *Kalanchoë* (Xu *et al.*, 2018). Subsidiary cells are believed to provide a reservoir of K⁺ and Cl⁻ ions for uptake into guard cells during stomatal opening and to act as a sink for these ions during stomatal closure (Willmer and Pallas, 1973). Confocal microscopy and mitochondrial staining indicated the distribution of chloroplasts and mitochondria within cell types found in the epidermis tissue sampled (Figure 1). Mitochondria were detected in both guard cells and subsidiary cells (Figure 1b,c), but chloroplasts were only detected within the guard cells (Figure 1b). Chloroplasts or mitochondria were not detected in the epidermal pavement cells. Epidermal peels stained with iodine showed starch deposits confined to chloroplasts in the guard cells (Figure 1d). This, together with the localization of autofluorescence in guard cells across the epidermis (Figure 1e), indicates negligible contamination of epidermal peels with chloroplasts from the underlying mesophyll.

Protein expression in *K. fedtschenkoi* epidermis and mesophyll

Some 41 504 non-redundant distinct peptide sequences were identified across the entire data set at a false discovery rate (FDR) of <1% at the peptide level, and those peptides mapped to 9102 *K. fedtschenkoi* proteins (Tables S1, S2). The high degree of protein sequence redundancy in plant proteomes (e.g. alternative transcription, protein families, etc.) leads to several proteins being identified by the

same set of tryptic peptides. To address this ambiguity, we assessed and report protein groups, which are created by clustering proteins together that are >90% similar in sequence identity. Overall, this approach resulted in an average identification of 5002 proteins and 2718 protein groups per epidermis sample, and an average of 3583 proteins and 1973 protein groups identified per mesophyll sample (Figure 2a). In general, there was an approximately 60% overlap in protein identifications between epidermis and mesophyll proteomes, with a substantially higher number of proteins unique to the epidermis when compared with the mesophyll (Figure 2b). Multivariate partial least squares (PLS) analyses found a clear distinction between the epidermis and mesophyll proteomes identified in the first component (Figure 2c) and a discrete grouping of the biological replicates. The average Pearson coefficient for biological reproducibility was 0.92 and 0.91 for the epidermis and the mesophyll, respectively. The average Pearson coefficient between the epidermis peel and the mesophyll was 0.74. Together, these general overviews indicate that the epidermis and the mesophyll have unique proteomes. Furthermore, there are underlying differences in the proteome across the diel period (PLS components 2 and 3), which has been observed in other CAM plants (Abraham *et al.*, 2016).

Across the proteins that were quantified, the dynamic range of the relative protein abundances spanned six orders in the epidermis and mesophyll proteomes, and in both proteomes a small fraction (approx. 3–4%) of the total proteins account for 50% of the total protein biomass (Figure S1a). We observed greater coverage of low-abundance proteins in the epidermis (Figure S1c), suggesting a more functionally diverse set of proteins expressed in this tissue compared with the mesophyll, which is dominated by proteins required for photosynthesis. As low-abundance proteins are sampled more stochastically, we implemented a limit of quantitation (LOQ) threshold to remove proteins accounting for <1% of the total observed protein intensity in the epidermis and mesophyll data sets (Table S3). Enforcing this criterion removed a substantial number of quantifiable proteins from the epidermis data set and had a lesser effect on the mesophyll data set (Figure S1b,d). The filtered data set will be used for all subsequent analyses because it allows for a more robust comparison of relative protein abundances between the epidermis and mesophyll data sets, where both have approximately the same number of quantifiable proteins.

High-abundance proteins have different functional roles in epidermis and mesophyll

The median protein abundance distributions of the epidermis and the mesophyll proteomes were characterized to identify the cellular processes and functions that are expressed at high protein abundance levels. When

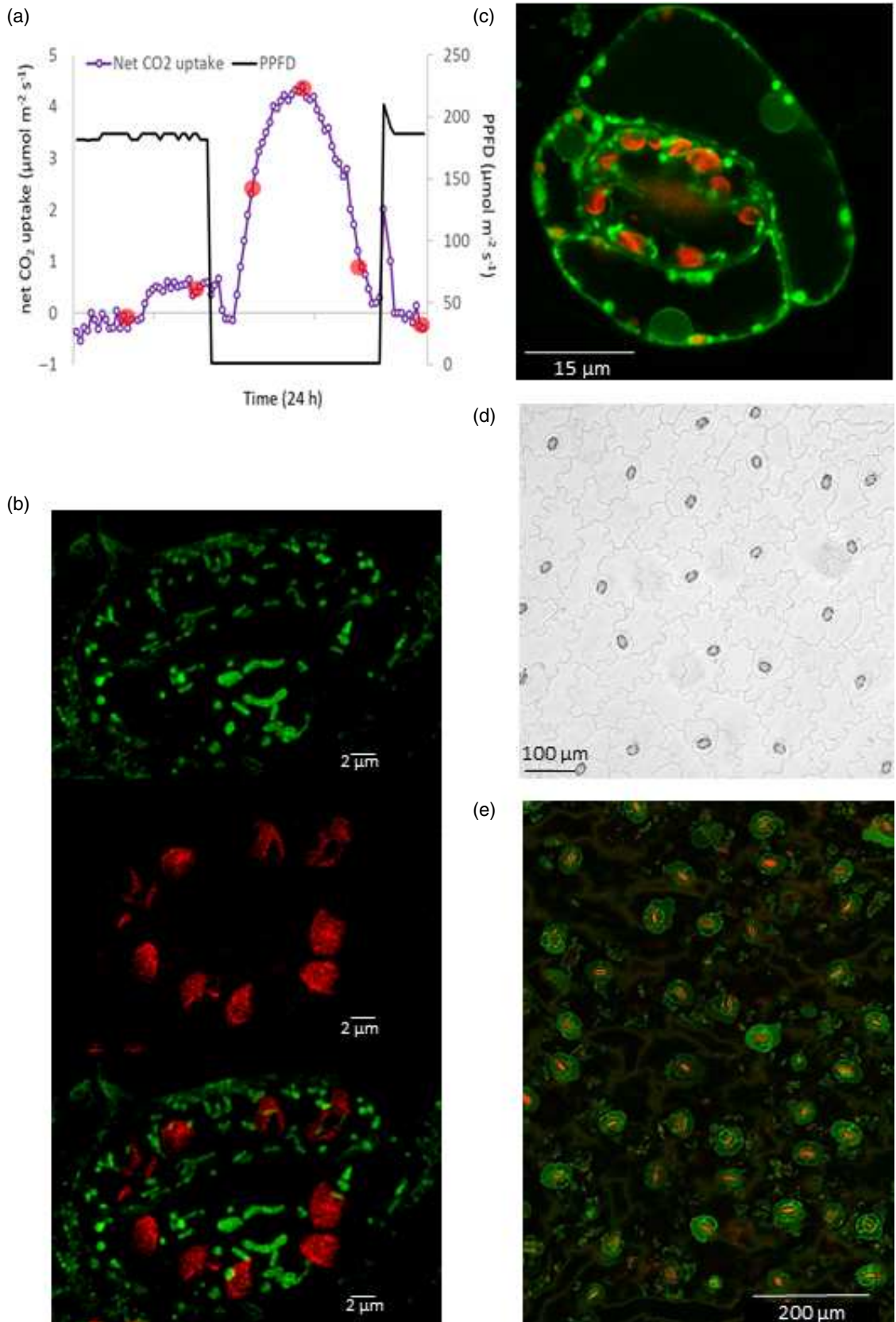


Figure 1. (a) Net CO₂ uptake (purple) and photosynthetic photon flux density (PPFD) (black) measured over the 24-h light/dark cycle for leaf 6 of *Kalanchoë fedtschenkoi* and indicating the time points used for sampling (with three biological replicates each) of mesophyll and epidermis: 00:00 h (dark), 04:00 h (dark), 08:00 h (dark), 12:00 h (light), 16:00 h (light), and 20:00 h (light). (b–d) Confocal microscopy images of epidermis where Rhodamine 123 staining indicates the presence of mitochondria (green staining) in both guard cells (b) and subsidiary cells (c), whereas autofluorescence (red coloring) of chlorophyll is evidence of chloroplast localization in guard cells (b, d). Iodine staining of epidermis shows the location of starch grains confined to guard cells and indicating negligible contamination from mesophyll chloroplasts (also seen in e). The epidermis was sampled from leaf pair 6 during the first 1–2 h of the photoperiod. Scale bars: 2 μm (b), 15 μm (c), 50 μm (d) and 200 μm (e).

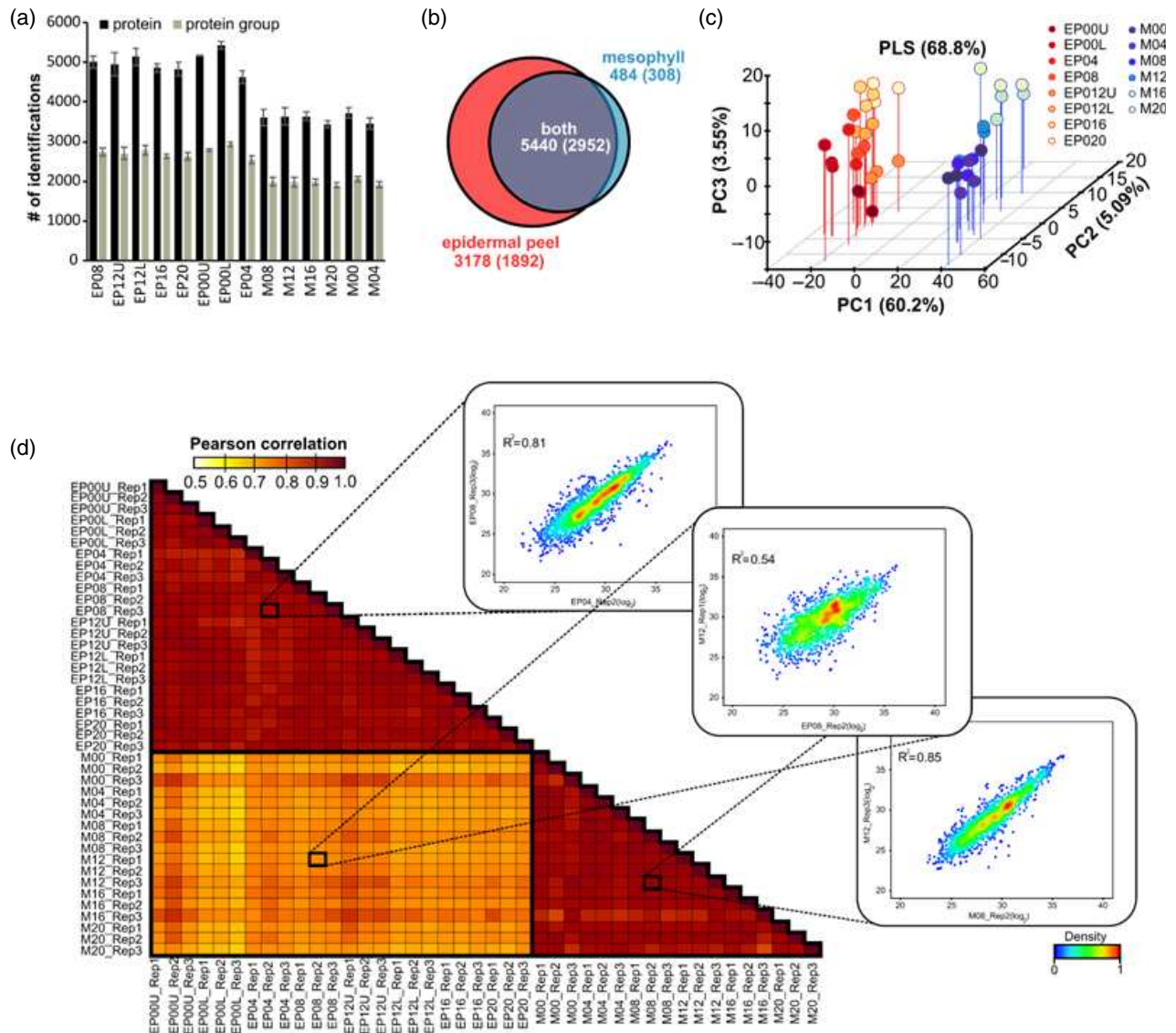


Figure 2. (a) Average number of identified proteins (black) and protein groups (grey) for the epidermis (EP) and mesophyll (M). For two time points, we measured an upper epidermal peel (EP12U and EP00U) and lower epidermal peel (EP12L and EP00L). Error bars represent the standard deviation across biological triplicates. (b) A Venn diagram illustrates the level of overlap observed in protein and protein group (in parentheses) identifications between the epidermis and mesophyll data sets. (c) Plot illustrating results from a three-component partial least squares (PLS) analysis. (d) A heat map contrast of calculated Pearson correlation coefficients to identify the level of similarity between samples across the entire experiment. Three companion scatterplots were arbitrarily chosen to provide a more detailed illustration of correlations in relative protein abundance between EP versus EP, EP versus M and M versus M.

logarithmically transformed (Figure S2a), distributions were similar between the epidermis and mesophyll data sets and the high-abundance proteins, 10th decile, contain

459 and 419 proteins, respectively. For the highest-abundance proteins within the epidermis data set, the gene ontology (GO) term 'response to cadmium ion' was the

most significantly enriched process observed, and other significantly enriched stress response-related terms had a higher representation of associated proteins in the epidermis compared with the mesophyll data set (Figure S2b). For the mesophyll cells, 'photosynthesis' was the most significantly enriched GO process and energy-related GO terms were more represented in the mesophyll 10th decile when compared with the epidermal data set. Overall, these results suggest that the top 10% most abundant proteins in the epidermis prioritize stress-response processes, a finding that supports the concept of the epidermis as the first point of contact for the perception of changes in aboveground environmental conditions.

Comparing relative protein abundances between epidermis and mesophyll

In total, 3313 proteins showed differences in abundance between the epidermis and mesophyll data sets (Figures S3 and S4; Table S4). We performed a GO enrichment test on proteins with higher relative abundances in the epidermis peel (Figure 3; Table S5) or in the mesophyll (Figure 4; Table S6), and summarize these findings in a network to highlight the major functional groups that were observed. For the epidermis, we identified 990 significantly enriched GO terms and used CLUEGO (Bindea *et al.*, 2009) to create a functionally organized GO term network that identified 11 major functional groups enriched in the epidermis

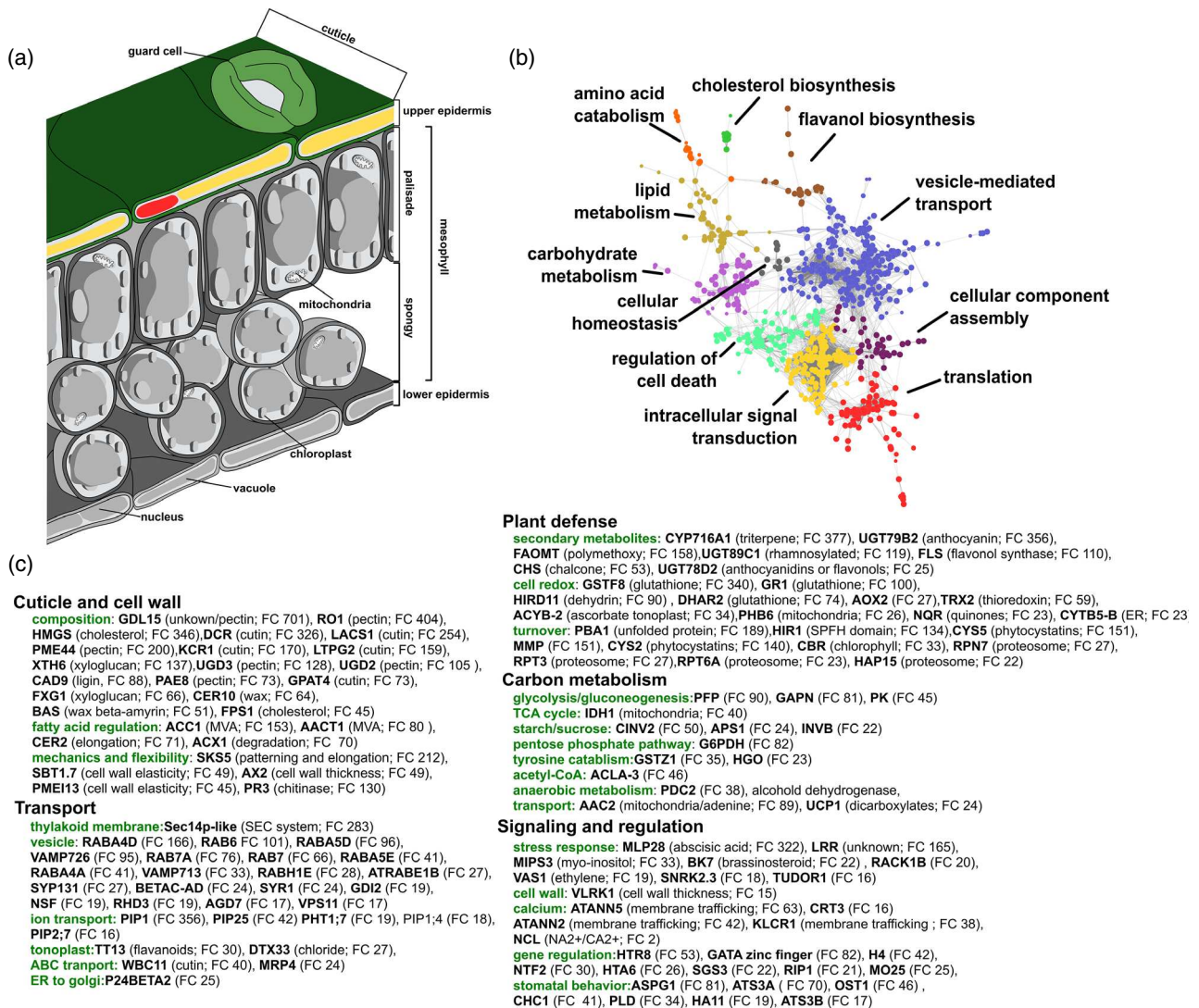


Figure 3. (a) Leaf diagram highlighting cells present in the epidermis proteome analysis. (b) CLUEGO network of gene ontology (GO) terms that were significantly enriched in the subset of proteins that were enriched in epidermal proteome. Each node represents an enriched GO term and edges represent functionally associated GO terms based on Kappa statistics. For each large subnetwork, major representative functions are shown. (c) A representative list of proteins and functional categories for the top 25% most significantly enriched proteins in the epidermis data set.

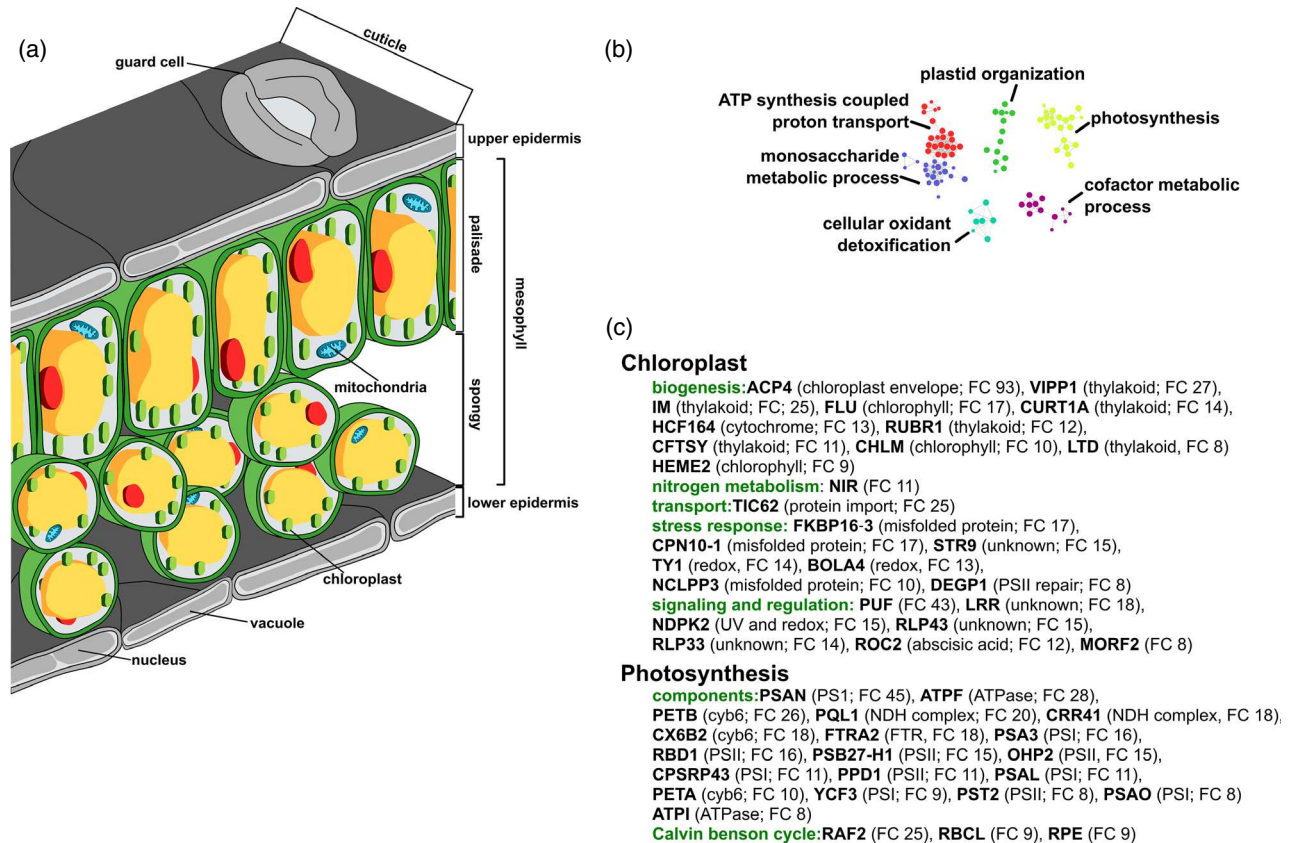


Figure 4. (a) Leaf diagram highlighting cells present in the mesophyll proteome analysis. (b) CLUEGO network of gene ontology (GO) terms that were significantly enriched in the subset of proteins that were enriched in the mesophyll proteome. Each node represents an enriched GO term and edges represent functionally associated GO terms based on Kappa statistics. For each large subnetwork, major representative functions are shown. (c) A representative list of proteins and functional categories for the top 25% most significantly enriched proteins in the mesophyll data set.

(Figure 3b). These included proteins involved in cuticle and cell-wall biosynthesis, transport, respiration, defense and signaling. At this high level, these functional modules are similar to those found expressed in the epidermis of other plants (Suh *et al.*, 2005; Mintz-Oron *et al.*, 2008). For proteins with significantly higher abundances on average in the mesophyll, we identified six major functional groups (Figure 4b). These included proteins involved in photosynthetic electron transport, photophosphorylation and ATP synthesis, the Calvin cycle, nitrogen metabolism and chloroplast biogenesis, and UV-related stress response proteins.

To provide a more detailed understanding of the proteins contained within these networks we manually interrogated the functional role and cellular implication for the top 25% most significantly enriched proteins identified between epidermis and mesophyll by leveraging resources from the TAIR database (Lamesch *et al.*, 2012) using BLAST (Mount, 2007) (Table S4). Information from the *A. thaliana* orthologs identified, and plausible functional roles for these proteins, are highlighted (Figures 3c and 4c).

In general, proteins involved in the biosynthesis of the cuticle and cell wall were found to have the highest abundance differences between the epidermis and the mesophyll proteomes (Figure 3c). The functional role of the protein with the greatest enrichment in the epidermis (GDL15, Kaladp0351s0002.1.p, fold change 701, $-\log_{10}$ *P* value 34.34, ortholog of AT1G29670.1), compared with the mesophyll, has been implicated in the catalysis of acyltransferase or hydrolase reactions with lipid and non-lipid substrates (Akoh *et al.*, 2004). We also identified several proteins with established roles in cuticle and cell wall formation, as well as proteins implicated in determining the biomechanical properties of the cell wall (Figure 3c).

Also enriched in the epidermis (Figure 3c) were proteins involved in the synthesis of secondary metabolites such as triterpenoids, phenylpropanoids and flavonoids, which are known to influence biotic interactions, have important medicinal (anti-inflammatory) properties in many species of *Kalanchoë* (Costa *et al.*, 2008) and can attenuate UV-B irradiation and heat damage (Hahlbrock and Scheel, 1989).

In general, carbon flux through mitochondria in the epidermis of *K. fedtschenkoi* appeared to be enhanced relative to that in the mesophyll, as indicated by significant enrichments in numerous mitochondrial proteins. These included diverse mitochondrial transport proteins, proteins of the tricarboxylic acid cycle (TCA) cycle and proteins required for the γ -aminobutyrate (GABA) shunt pathway, which provides an alternative carbon source for the TCA cycle, particularly if pyruvate supply becomes limiting (Bouche and Fromm, 2004). Mitochondria are concentrated within the guard cells and subsidiary cells of the *K. fedtschenkoi* epidermis. Thus, like the stomata of C_3 plants, CAM stomata are similarly set up to supply extra energy for guard cell metabolism and ion fluxes via increased capacity for oxidative phosphorylation (Fricker and Willmer, 1996; Araujo *et al.*, 2014).

Enhanced respiratory activity in the epidermis relative to the mesophyll was also supported by the enrichment of proteins implicated in cell redox homeostasis in the epidermis (Figure 3c). Of these, the protein with the greatest fold change in epidermis relative to mesophyll was a glutathione *S*-transferase (GSTF8, Kaladp0044s0060.1.p, fold change 340, $-\log_{10} P$ value 28.48, ortholog of AT2G47730). This protein also showed dynamic diel changes in abundance in the epidermis, peaking in the middle of the photoperiod (Figure 5, cluster 4). A chloroplastic location for this GST ortholog in *K. fedtschenkoi* implies a potential role in guard cell redox metabolism and/or signaling.

Several plasma membrane intrinsic proteins (PIPs) were found to be significantly enriched in the epidermis relative to the mesophyll of *K. fedtschenkoi* (e.g. PIP1:4, Kaladp0959s0007.1.p, fold change 110, $-\log_{10} P$ value 9.05,

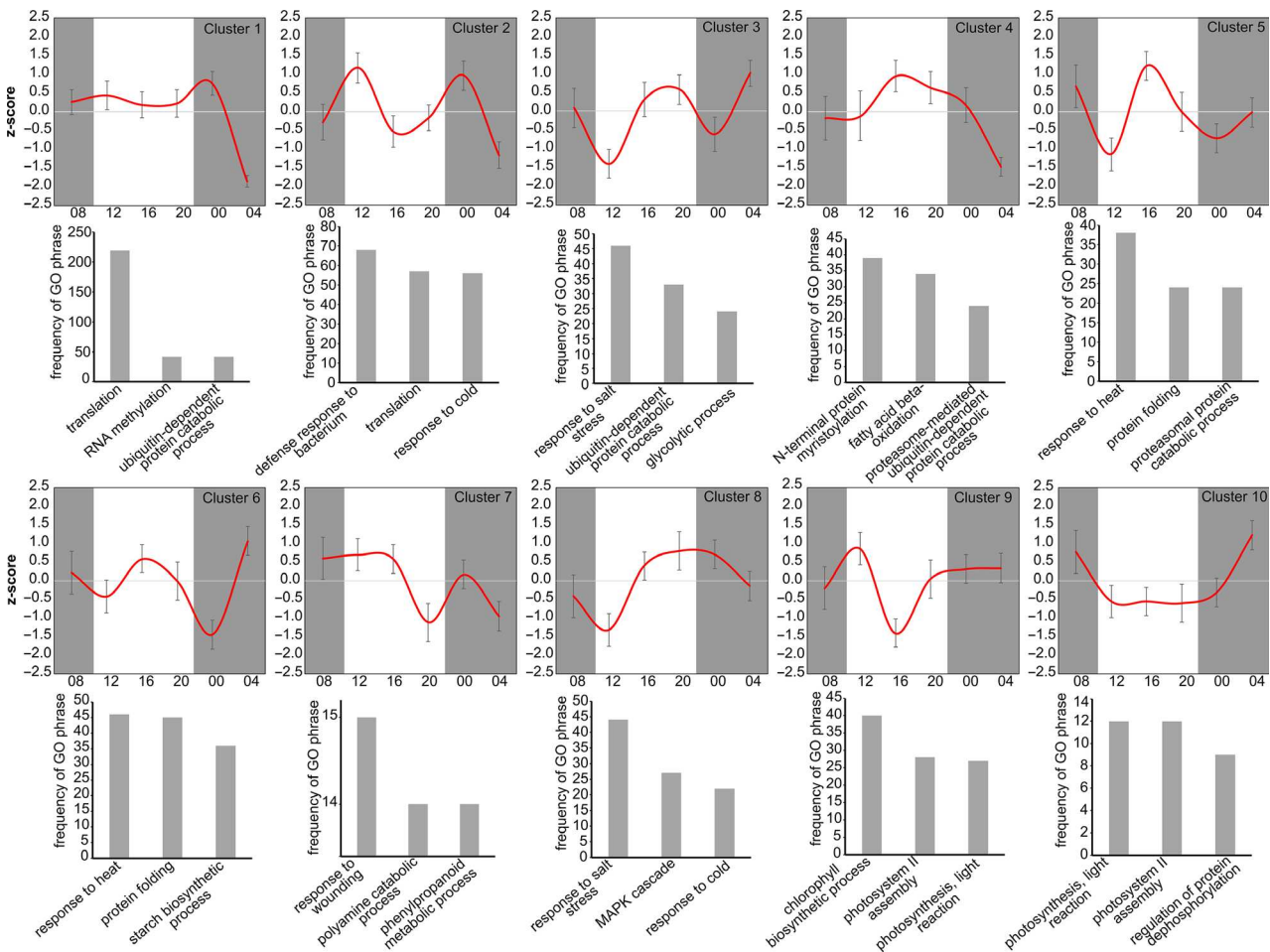


Figure 5. Temporal changes in protein abundances across the diel cycle in epidermis.

k-means clustering grouped proteins into 10 clusters based on the similarity of their abundance profiles. The y -axis represents the average z -score for each protein [(abundance – mean)/standard deviation] and highlights prominent patterns of abundance across the diel cycle. Error bars represent the \pm standard deviation of the mean ($n = 3$) of protein abundance trends within each cluster. Below each cluster, the top three most frequent significant gene ontology terms are graphically represented.

ortholog of AT4G0043; PIP2:5, Kaladp0099s0104.1.p, fold change 41, $-\log_{10}$ *P* value 13.86, ortholog of AT3G54820). PIPs are crucial for mediating the hydraulic flow necessary for stomatal opening (Oparka and Roberts, 2001) and can also enhance the permeability of CO₂ across the plasma membrane and the chloroplast envelope, thereby increasing the effectiveness of rubisco and potentially influencing transpiration efficiency (Heinen *et al.*, 2009; Groszmann *et al.*, 2017).

Stomatal regulation and signaling in the epidermis proteome. Among the proteins most enriched in the epidermis compared with the mesophyll, we identified several proteins with known roles in regulating stomatal behavior (Figure 3c). These included a number of membrane-localized transporters such as PLASMA MEMBRANE PROTON ATPases (PMA11). Of particular interest were *K. fedtschenkoi* orthologs of AHA2 and AHA8, which peaked in protein abundance towards the end of the photoperiod and over the first part of the night (Figure 5, cluster 8; Table S4). In *Arabidopsis*, AHA1 and AHA2 induce the hyperpolarization of the guard cell plasma membrane and allow K⁺ uptake through inward-rectifying K⁺ channels, thereby inducing guard cell swelling and stomatal opening (Ueno *et al.*, 2005). The diel patterns of protein abundance for the *K. fedtschenkoi* AHA orthologs described here suggest a key role for these proteins in mediating nocturnal stomatal opening, which requires future functional analysis. Proteins implicated in guard cell signaling that were enriched in the epidermis included orthologs of phospholipase D (PLD) and aspartic protease (ASPG1), which function through abscisic acid (ABA) signaling in guard cells (Yao *et al.*, 2012). We also identified orthologs of several calcium signaling proteins that were enriched in the *K. fedtschenkoi* epidermis (Figure 3c; Table S4). In particular, an ortholog of CPK21 (AT4G04720.1, Kaladp0040s0351.1.p, fold change 8, $-\log_{10}$ *P* value 10.94) showed a diel change in abundance, peaking during the day (Figure 5, cluster 1). In *Arabidopsis*, CPK21 has been shown to mediate the phosphorylation and activation of the S-type anion efflux channel SLAC1, which mediates stomatal closure (Geiger *et al.*, 2010). The elevated protein abundance of this ortholog during the day in the epidermis of *K. fedtschenkoi* highlights a possible role for calcium-dependent protein kinases in mediating the daytime stomatal closure that defines CAM.

An ortholog of the sucrose non-fermenting receptor kinase 2.6, also known as Open Stomata 1 (OST1), was detected in the epidermis (but not in the mesophyll) of *K. fedtschenkoi* (Table S4). OST1 is activated in the presence of ABA and promotes anion and water efflux, the inhibition of K⁺ influx and stomatal closure (Grondin *et al.*, 2015). In the CAM species *A. americana* and *K. laxiflora*, OST1 exhibits a diel rescheduling of transcript abundance

to the day, compared with the night in *Arabidopsis* (Abraham *et al.*, 2016; Boxall *et al.*, 2020), consistent with a putative role for this protein in stomatal closure. The OST1 protein in *K. fedtschenkoi* did not show any detectable change in diel abundance, however. This finding reinforces the view that diel changes in transcript abundance do not necessarily reflect a change in protein abundance or activity. Future interrogation of this proteomics data set alongside complementary transcriptomics data sets for the *K. fedtschenkoi* epidermis will be valuable for revealing the layers of transcriptional and post-transcriptional control of membrane transport and signaling components that underpin CAM stomatal behavior.

Diel protein abundance profiles in epidermis and mesophyll

Crassulacean acid metabolism (CAM) differs from C₃ and C₄ photosynthesis in terms of the diel rescheduling of metabolism and stomatal regulation, so we sought to provide a proteome-wide perspective on which proteins display significant changes in their diel abundance profiles. We used *k*-means clustering to capture orchestrated co-abundance responses in the epidermal and mesophyll proteomes. We identified 691 and 371 protein abundance patterns in the epidermal peel and mesophyll proteomes, respectively, with *P* < 0.05, that showed at least a twofold change between two time points across the diel cycle (Tables S7 and S8). Using *k*-means and the gap statistic method (Tibshirani *et al.*, 2001), proteins were grouped into 10 and 14 major clusters based on the similarity of expression patterns identified for the epidermal (Figure 5) and mesophyll (Figure 6) data sets, respectively. To detect functional specialization within each cluster, we cross-referenced the top protein blast result with its corresponding entry in the TAIR gene ontology database and quantified the frequency of each GO phrase using controlled vocabularies, where frequency refers to the number of phrases in each cluster (Berardini *et al.*, 2004) (Tables S9 and S10). The three most over-represented GOs for each cluster are shown in Figures 5 and 6.

For the epidermis, the largest protein cluster consisted of proteins with a significant decrease in abundance during the middle of the night (Figure 5, cluster 1). Within this cluster, 'translation' and 'RNA methylation' were the top two most represented GO groups, and we also observed many ribosomal proteins (*n* = 24), suggesting an enhanced protein turnover in the epidermis, which may be linked to high respiratory activity and the turnover of reactive oxygen species (ROS) in this tissue, as discussed above. A key aim was to provide insight on cellular behavior underpinning CAM stomatal behavior. Proteins within epidermal cluster 8, which showed abundance patterns that anticipated late photoperiod and nocturnal opening of stomata (Figure 1a), were of particular interest. The most

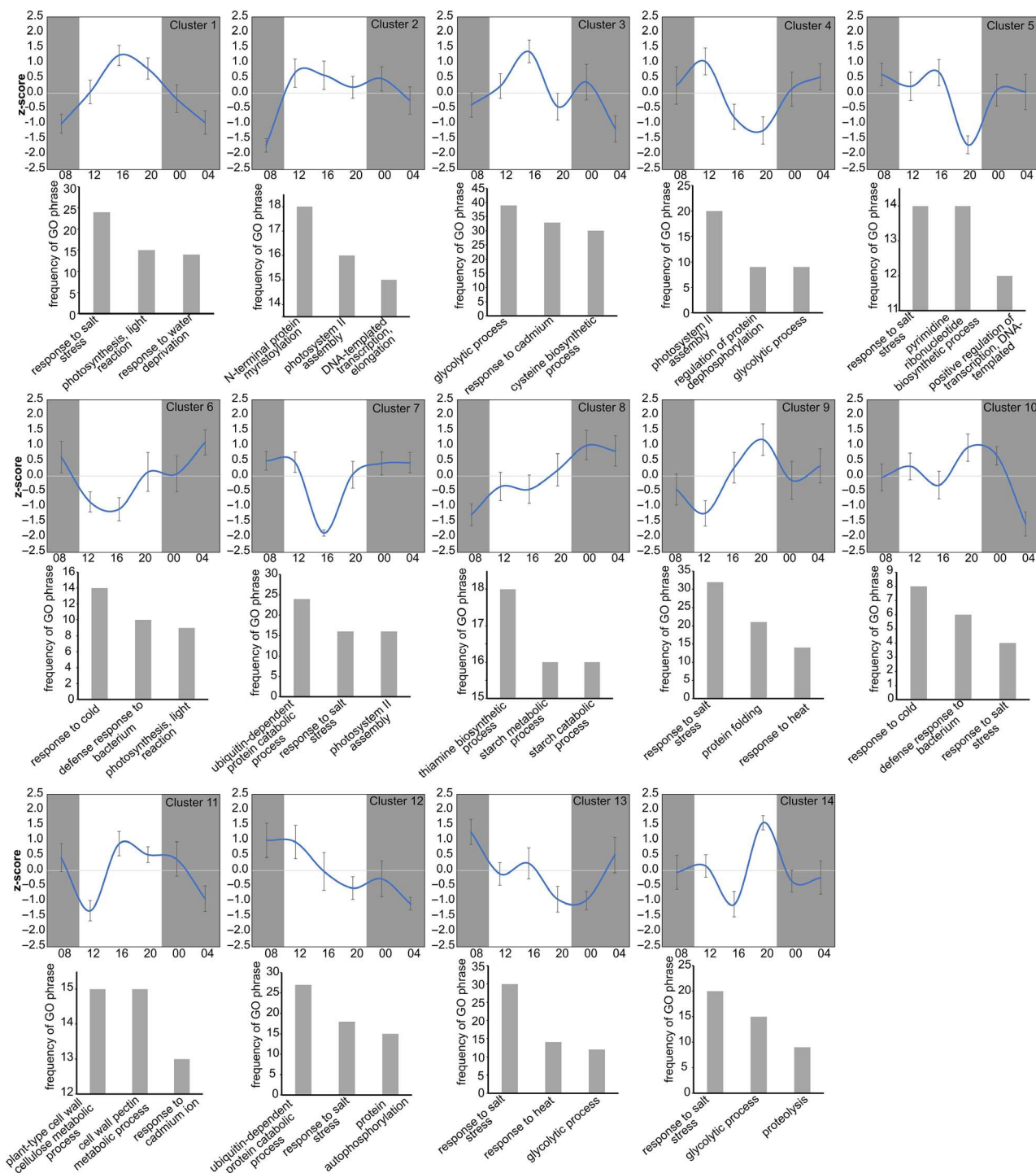


Figure 6. Temporal changes in protein abundances across the diel cycle in mesophyll. *k*-means clustering grouped proteins into 14 clusters based on the similarity of their abundance profiles. The *y*-axis represents the average z-score for each protein [(abundance – mean)/standard deviation] and highlights prominent patterns of abundance across the diel cycle. Error bars represent the \pm standard deviation of the mean ($n = 3$) of protein abundance trends within each cluster. Below each cluster, the top three most frequent significant gene ontology terms are graphically represented.

represented GO groups within cluster 8 were ‘response to salt stress’ and ‘MAPKinase cascade’, and the most represented GO locations within this cluster were the plasma

and vacuolar membranes. Proteins found within this cluster included several plasma membrane proton ATPases, including orthologs of AHA2 and AHA8, vacuolar proton

pyrophosphatases (orthologs of AVP1, AT1G15690), a vacuolar proton ATPase (ortholog of VHA, AT4G23710) and a putative voltage-gated potassium channel subunit (ortholog of KAB1, AT1G04690). The diel patterns of abundance of these proteins is consistent with the hypothesis that stomatal opening towards the end of the day and into the night requires the energization of plasma membrane and tonoplast proton pumps, as well as the activation of pathways for K⁺ uptake at the plasma membrane and tonoplast. Also found within cluster 8 were several MAP kinases (Kaladp0046s0065.1 and Kaladp0046s0065.3, orthologs of AT4G29810). MAP kinase signaling cascades have been implicated in CO₂ signal transduction for stomatal movement in Arabidopsis (Zhang *et al.*, 2018). The proteins described above, together with others found within cluster 8, which include proteins implicated in sphingolipid metabolism, RAS-related GTP binding and mitochondrial respiratory electron transport, represent important candidates for future functional testing of signaling and metabolic pathways, as well as ion transporters important for CAM stomatal regulation.

The major temporal cluster for the mesophyll proteome contained proteins that increased in abundance during the day and decreased during the night (Figure 6, cluster 1). The most represented GO groups within this cluster were 'response to salt stress', 'photosynthesis light reactions' and 'response to water deprivation'. In general, this cluster included proteins belonging to photosystems, light-harvesting complexes, the maintenance of transmembrane electrochemical gradients, the Calvin–Benson cycle and photorespiration, as well as heat-shock proteins. Cluster 6 contained mesophyll proteins that showed a reciprocal diel pattern of protein abundance to that of cluster 1, i.e. proteins that showed the greatest abundance during the night. The most represented GO groups within this cluster included stress-responsive proteins, proteins implicated in defense and, intriguingly, in the light reactions of photosynthesis. Of particular note were proteins implicated in redox homeostasis (e.g. glutathione peroxidase, thioredoxin and ferredoxin). This finding supports the emerging view of the need for antioxidant activity to deal with the ROS generated by high rates of respiratory electron transport that occur at night in CAM plants (Abraham *et al.*, 2016; Shameer *et al.*, 2018).

Characterization of proteins implicated in the diel carboxylation and decarboxylation processes of CAM

A key aim of our study was to explore the hypothesis of tissue-specific regulation of metabolic processes underpinning diel turnover of malate and starch within the mesophyll and the epidermis. To provide context for these analyses we measured diel changes in malate (Figure 7a), as well as starch, in both mesophyll and epidermal peels (Figure 7b). Nocturnal accumulation and daytime

mobilization of malic acid was evident in the mesophyll as well as in the epidermis peel, but on a fresh-weight basis, diel turnover of malate was over eight times higher in the mesophyll cells compared with the epidermal peels.

To sustain nocturnal CO₂ uptake and malic acid accumulation, *K. fedtschenkoi* mobilizes starch for the nocturnal provision of PEP, and within the mesophyll starch was steadily and almost completely degraded overnight and subsequently resynthesized during the day (Figure 7b). Substantial starch deposits were observed within the guard cells of *K. fedtschenkoi* (Figures 1 and 7b), but diel turnover of guard cell starch was significantly dampened compared with that of the mesophyll cells (Figure 7b). Importantly, the daytime accumulation of starch within the guard cells of *K. fedtschenkoi* is in marked contrast to that reported for the C₃ model Arabidopsis, where starch in guard cells is broken down almost completely within the first hour of the photoperiod, potentially to generate malate and/or sugars, which provide the energy and osmolytes required to open C₃ stomata at the start of the day (Horrer *et al.*, 2016). Studies have shown that gluconeogenesis-mediated starch synthesis removes malic acid from guard cells, which can promote stomatal closure (Schnabl, 1980). Although the localization of malate in the epidermal peels cannot be definitely reconciled to the guard cells, the observed reciprocal relationship between daytime starch accumulation in the guard cells and daytime depletion of malate in the epidermis (Figure 7) is consistent with this hypothesized role for starch and malate metabolism in stomatal regulation.

Distribution of proteins responsible for C₄ carboxylation between epidermis and mesophyll. Many of the proteins required for CAM are encoded by multigene families, suggesting that different isoforms responsible for nocturnal carboxylation and daytime decarboxylation might carry out specific roles within the mesophyll and epidermis, with those isoforms present in the epidermis having implications for stomatal regulation (Figure S5). β-Carbonic anhydrase (BCA) catalyzes the hydration of CO₂ to HCO⁻, the substrate for nocturnal carboxylation in CAM. The most abundant protein accessions of BCA in mesophyll and epidermis were Kaladp0018s0289.1.p, ortholog of Arabidopsis BCA2, and Kaladp0538s0011.1.p, ortholog of Arabidopsis BCA1. The *kf*BCA1, which has been previously reported as the CAM-specific BCA on the basis of increased transcript abundance at night (Yang *et al.*, 2017), showed significant diel changes in protein abundance in the epidermis (Figure 5, cluster 2) but not in the mesophyll. A third *kf*BCA (Kaladp0081s0140, ortholog of BCA5 in Arabidopsis) was only detected in the epidermis and had a protein abundance pattern that peaked in concert with the maximal rates of nocturnal net CO₂ uptake and stomatal conductance (Figures 1 and S5). This *kf*BCA5 is predicted to

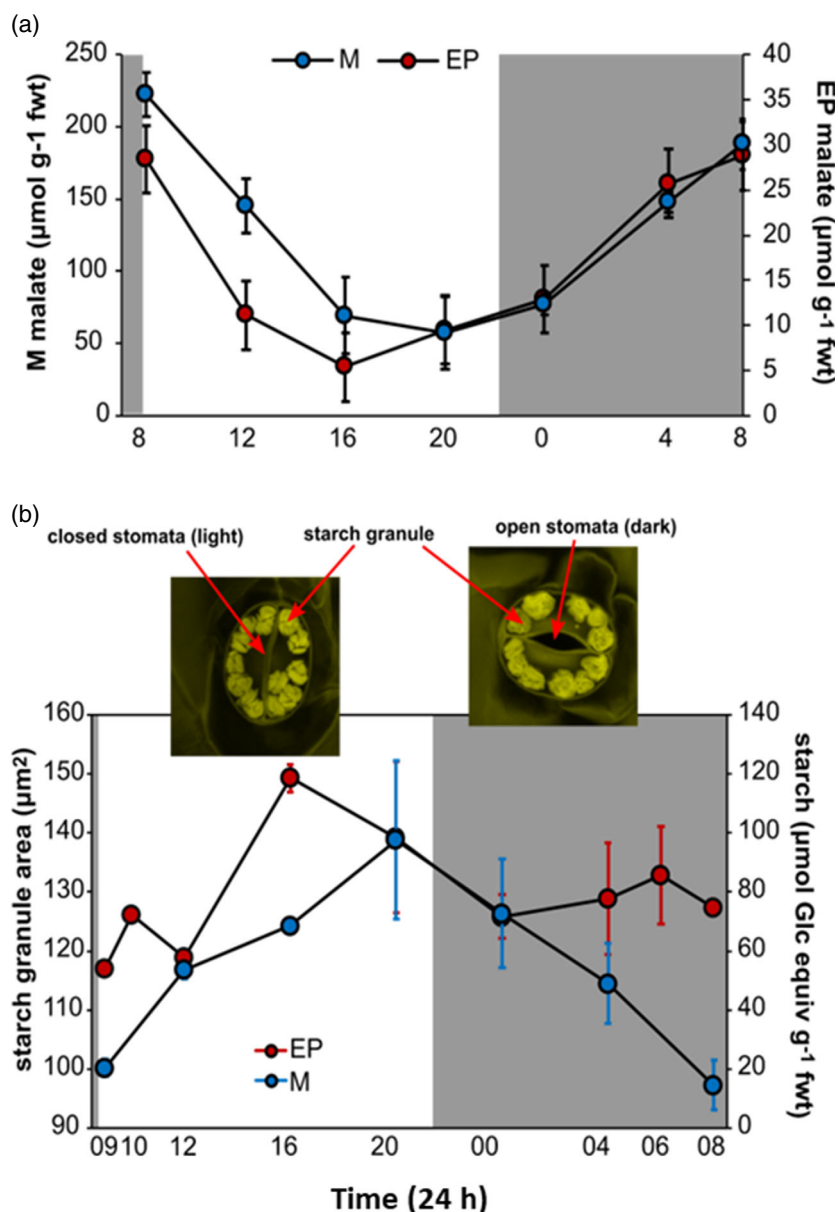


Figure 7. (a) Day/night changes in malate content in the epidermis and mesophyll; (b) quantification of starch content within the guard cells as starch granule area for epidermal peels taken from the upper leaf surfaces. Fluorophore propidium iodide and confocal laser scanning microscopy illustrate starch granules within closed (day) and opened (night) stomata. Day/night changes in starch content measured in leaf mesophyll following enzymatic digestion and colorimetric assay determination. Each point is the mean of three biological replicates \pm standard deviation of the mean.

localize to the chloroplast and thus the guard cells of *K. fedtschenkoi*. In *Arabidopsis*, mathematical modelling has indicated a central role for guard cell-localized BCAs in mediating intracellular HCO_3^- concentration change, which is a key mechanism in mediating CO_2 -regulated stomatal movement (Hu *et al.*, 2010; Hu *et al.*, 2015). Further functional testing is required to establish whether the epidermal-enriched *kfBCA5* isoform has a role in mediating the diel changes in stomatal movement that accompany the substantial changes in pCi across the day/night phases of CAM.

Phosphoenolpyruvate carboxylase catalyzes the carboxylation of PEP, which leads to nocturnal CO_2 uptake and malate accumulation. The PEPC protein accession with the highest relative abundance in both tissues

(Kaladp0095s0055.1.p) matches the PEPC1 protein sequence in *K. laxiflora*, which is essential for CAM (Boxall *et al.*, 2020) (Figure S5). For all the *kfPEPC* proteins identified, we did not observe significant differences in abundance between the epidermal and mesophyll proteomes. We identified phosphorylation modifications for the most abundant *kfPEPC1* protein, which confirmed the same phosphorylation modification at the N-terminus (Ser-13) in both the epidermal and mesophyll data set (Figure 8; Table S11). Averaging the relative abundance of the phosphopeptides identified revealed that *kfPEPC1* is phosphorylated during the night and dephosphorylated during the day in both the mesophyll and epidermis proteomes. This diel pattern of PEPC phosphorylation, which is the inverse of that found in C_3 plants, is critical for the temporal/

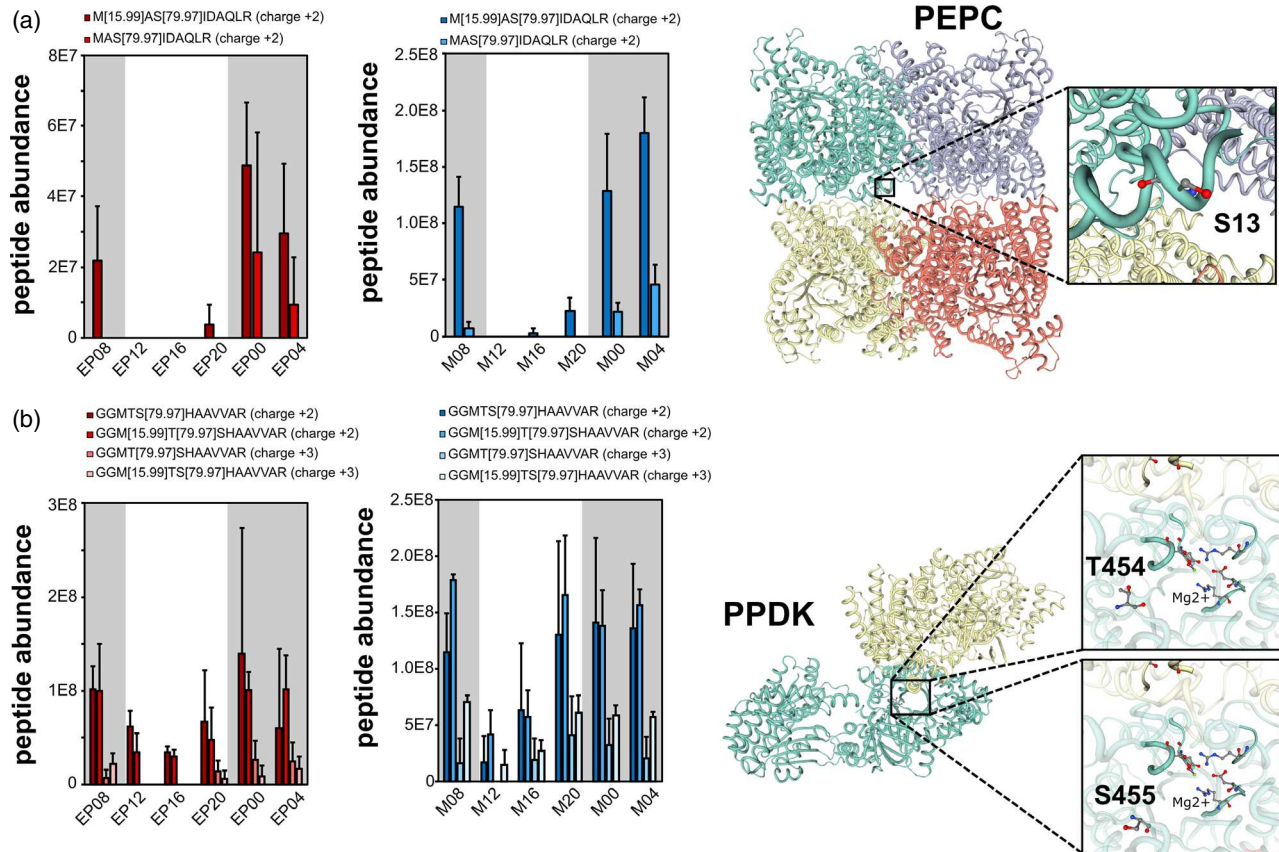


Figure 8. Phosphorylation of phosphoenolpyruvate carboxylase (PEPC) and Pyruvate orthophosphate dikinase (PPDK). (a) For each time point, the average relative abundance of all identified phosphopeptide variants (i.e. sequence, post-translational modifications and charge state) for PEPC are illustrated for the epidermis (red) and mesophyll (blue) data sets. The error bars represent the standard variation across three biological replicates. The amino acid position on each peptide for localized phosphorylation modifications (79.97; STY) and methionine oxidation (15.99; M) are shown. (b) Homology-model structure for PEPC with the localized phosphorylation site at Ser-13 near the center of the homotetramer. (c) For each time point, the average relative abundance of all identified phosphopeptides variants (i.e. sequence, post-translational modifications, and charge state) for PPDK are illustrated for the epidermis (red) and mesophyll (blue) data sets. The error bars represent the standard variation across the three biological replicates. The amino acid position on each peptide for localized phosphorylation modifications (79.97; STY) and methionine oxidation (15.99; M) are shown. (d) Homology-model structure for PPDK with the localized phosphorylation sites at Thr-454 and Ser-455.

circadian control of carboxylation processes operating within the leaf mesophyll of CAM plants (Boxall *et al.*, 2017). Nocturnal phosphorylation of PEPC in the CAM stomatal complex, as indicated by our data, is in marked contrast to the daytime phosphorylation of PEPC reported for C₃ guard cells (Wang *et al.*, 1994), and could protect the CAM enzyme against inhibition by malate during guard cell swelling and stomatal opening at night.

Distribution of proteins responsible for malate decarboxylation between mesophyll and epidermis. Daytime decarboxylation of malate in the mesophyll of *K. fedtschenkoi* is catalyzed by mitochondrial NAD malic enzyme (Dever *et al.*, 2015). Protein accessions for several isoforms of NAD-ME were identified (Kaladp0033s0124.1.p, ortholog of AT2G13560.1 NAD ME1; Kaladp0037s0467.1.p ortholog of AT4G00570.1 NAD ME2): *kfNAD* ME1 had comparable abundance in the mesophyll and the epidermis, but *kfNAD*

ME2 was significantly more abundant in the epidermis (Figure S5). Diel changes in *kfNAD* ME1 and *kfNAD* ME2 abundances were only evident in the mesophyll (clusters 4 and 13, Figure 6), and increased *kfNAD* ME1 abundance in the middle of the day corresponded with the period of maximal malate decarboxylation. Both *kfNAD* ME1 and *kfNAD* ME2 also peaked in abundance over the latter part of the dark period, which could indicate the breakdown of malate to provide pyruvate for mitochondrial respiration at night (Holtum *et al.*, 2005).

Protein accessions for cytosolic/chloroplastic NADP ME were also identified (Kaladp0046s0046.2.p, Kaladp0102s0114.1.p and Kaladp0024s0016.1.p, orthologs of AT5G25880.1 and NADP-ME3, and Kaladp0092s0166.1.p and Kaladp0045s0427.1.p, orthologs of AT1G79750.1 and NADP-ME4; Table S4); all of these were more abundant in the epidermis, suggesting functional diversification in malate metabolism within the cells of the epidermis

compared with the mesophyll. In addition to a role in CAM-related malate turnover, cytosolic NADP-MEs can control cytosolic pH (Martinoia and Rentsch, 1994; Lai *et al.*, 2002) and turgor pressure in guard cells (Outlaw *et al.*, 1981; Maurino *et al.*, 1997; Laporte *et al.*, 2002), whereas chloroplastic NADP-ME has been implicated in lipid biosynthesis (Wheeler *et al.*, 2005). Together, our data highlight contrasting roles for specific NAD and NADP ME isoforms in the CAM mesophyll and epidermis.

Distribution of proteins responsible for pyruvate processing between mesophyll and epidermis. Pyruvate orthophosphate dikinase (PPDK) converts pyruvate generated from malate decarboxylation back to PEP for subsequent gluconeogenic processing and the production of sucrose and/or starch. We identified protein accessions for two PPDKs: Kaladp0076s0229 (ortholog of AT4G15530) and Kaladp0039s0092 (ortholog of AT4G15530), with Kaladp0076s0229 having enriched abundance within the mesophyll (Figure S5). PPDK activity in *K. fedtschenkoi* is subject to post-translational control via reversible phosphorylation (Dever *et al.*, 2015). Phosphopeptide abundance in the most abundant PPDK protein indicated that the phosphorylation site was localized to a target residue, Ser-455 and/or Thr-454, similar to the target location of dephosphorylation/phosphorylation of PPDK in the *C₄* species *Zea mays* (Thr-456) (Figure 8; Table S11) (Chastain *et al.*, 1997). The diel pattern of phosphopeptide abundance we observed is consistent with a previous report of phosphorylation/inactivation of PPDK during the dark in *K. fedtschenkoi* (Dever *et al.*, 2015), although diel changes in phosphopeptide abundance were more marked in PPDK from the mesophyll, compared with epidermal PPDK (Figure S5). PPDK phosphorylation is catalyzed by PPDK regulatory protein (PPDK RP), an ortholog of which was significantly more abundant in the mesophyll (Kaladp0060s0363.1.p, fold change 9.4, $-\log_{10}$ *P* value 4.91). This PPDK-RP showed increased diel abundance at the end of the photoperiod and for most of the dark period (Figure 6, cluster 9), which is consistent with diel changes in phosphorylation/inactivation of PPDK required for CAM. Together, the data suggest that the enzymatic capacity for daytime recovery of PEP from malate decarboxylation are higher in the mesophyll compared with the epidermis of *K. fedtschenkoi*.

Our data highlight other differences between the mesophyll and the epidermis in terms of pyruvate processing (Figure S6). Pyruvate kinase (PK) catalyzes the final reaction of the glycolytic pathway, converting ADP and PEP to ATP and pyruvate; an ortholog of cytosolic PK (Kaladp0039s0147.2.p, fold change 45, $-\log_{10}$ *P* value 19.35, ortholog of AT5G56350.1) was significantly enriched in abundance in the epidermis. Elevated PK activity in the epidermis implies enhanced pyruvate supply to mitochondria

for ATP production in the subsidiary and guard cells, compared with that in the mesophyll, whereas reduced activity of PK in the CAM mesophyll at night would be important for directing glycolytic flux towards PEP as a substrate for PEPC (Holtum *et al.*, 2005). Further indication of the importance of pyruvate metabolism in the epidermis of *K. fedtschenkoi* is indicated by marked diel abundance changes in pyruvate decarboxylase (PDC2, Kaladp0055s0499.1.p, ortholog of AT5G54960), a protein heavily enriched in the epidermis (Figure S6). In *C₃* plants, PDC has been implicated in drought tolerance by stimulating the jasmonate (JA) signaling pathway (Kim *et al.*, 2017). The diel abundance pattern of PDC in *K. fedtschenkoi* is similar to that observed for the PDC2 protein ortholog in the CAM species *A. americana* (Abraham *et al.*, 2016), suggesting an important role for PDC in CAM that requires further testing.

Distribution of proteins implicated in diel starch turnover between mesophyll and epidermis. We also probed whether contrasting functions for starch turnover in the mesophyll and the guard cells of *K. fedtschenkoi* would be reflected in the profiles of proteins implicated in starch metabolism within the two proteomes (Figure S7). The most abundant starch degrading protein in both mesophyll and epidermis proteomes was an ortholog of plastidic α -glucan phosphorylase (PHS1). This finding is consistent with suggestions that CAM shows a re-routing of chloroplastic starch degradation from the *C₃* amylolytic route to the phosphorylytic route catalyzed by PHS1, which can result in the production and export of glc-6-P from the CAM chloroplast (Borland *et al.*, 2016; Shameer *et al.*, 2018; Ceusters *et al.*, 2019). Orthologs of α -amylases 1 and 3 (AMY1 and AMY3) were also found with comparable abundances in the mesophyll and the epidermis. Studies on *Arabidopsis* have indicated that although AMYs are not essential for starch degradation in the leaf mesophyll, in the guard cells starch degradation is mediated by AMY3 acting in conjunction with β -amylase 1 (BAM1) (Horrer *et al.*, 2016). Two BAM orthologs, BAM2 and BAM9, were detected in the *K. fedtschenkoi* proteome. BAM9 was the most abundant BAM in both the epidermis and the mesophyll and showed a distinctive diel change in abundance in both the mesophyll and the epidermis, with the peak abundance noted in the middle of the night. Evidence for a catalytic role for BAM9 is currently lacking but a regulatory role in starch degradation has been suggested (Monroe and Storm, 2018). BAM2 was only detected in the epidermal proteome and showed a strong diel change in abundance, peaking towards the end of the photoperiod coincident with the timing of guard cell starch degradation (Figure 7b). BAM2 was recently shown to be catalytically active in the presence of physiological concentrations of KCl in

Arabidopsis (Monroe *et al.*, 2018), suggesting a possible role in guard cell starch degradation.

Two proteins implicated in the cytosolic processing of starch degradation products showed significantly higher abundance in the *K. fedtschenkoi* epidermis compared with the mesophyll (Figure S7). In *Arabidopsis* mesophyll cells, the amylolytic breakdown of starch in the chloroplast produces maltose, which is exported and metabolized via a transglucosylation reaction catalyzed by disproportionating enzyme 2 (DPE2). This reaction produces a cytosolic heteroglycan intermediate, which is acted on by cytosolic α -glucan phosphorylase (PHS2) to produce glc-1-P (Malinova and Fettke, 2017). The elevated abundance of the *K. fedtschenkoi* orthologs of DPE2 and PHS2 in the epidermis provides further indication of a possible divergence in the route and regulation of starch breakdown in the guard cells and mesophyll of this CAM species.

Sustained accumulation of guard cell starch in *K. fedtschenkoi* over the first part of the photoperiod is in marked contrast to the almost complete mobilization of starch in *Arabidopsis* guard cells at the start of the day. The substantial starch deposits found in the CAM guard cells imply a critical role for starch synthesis in CAM stomatal function. An analogy can be found in the suggestion that in *Arabidopsis*, guard cell starch synthesis plays an essential role in CO₂-induced stomatal closure by acting as a sink for C-skeletons coming from malate degradation via gluconeogenesis during guard cell osmotic adjustment (Azoulay-Shemer *et al.*, 2016). We compared proteins implicated in gluconeogenesis and starch synthesis between epidermal and mesophyll proteomes and identified an ortholog of pyrophosphate-dependent phosphofructokinase (PFK), which showed an above-average relative abundance in the epidermal proteome yet was not detected in the mesophyll (Figure S6). Acting in the direction of gluconeogenesis, PFK provides Fru-6-P for conversion to Glc-6-P, which could be imported to the guard cell chloroplast via the plastidic glc-6-P translocator (GPT) for subsequent starch synthesis via ADP glucose pyrophosphorylase (AGPase). Further work is required to establish the functional significance of the proteins identified above in terms of guard cell starch metabolism and CAM stomatal function.

CONCLUSION

This study provides a quantitative understanding of biological phenomena occurring at the protein level in guard cell-enriched epidermis and mesophyll from leaves of the constitutive model CAM plant *K. fedtschenkoi*. Our data indicate tissue-specific specialization of isozymes implicated in malate and pyruvate processing and in starch turnover. These findings are discussed in line with contrasting roles for these metabolites within the CAM mesophyll and stomatal complex. A key finding to emerge was the diel rescheduling of guard cell starch turnover in *K. fedtschenkoi* compared

with that observed in *Arabidopsis*. Growing recognition of the importance of primary carbon metabolism in regulating stomatal movements in C₃ plants (Santelia and Lawson, 2016) indicates a pressing need for a better understanding of metabolism within CAM guard cells. In turn, such information will be essential for establishing whether the bioengineering of CAM into non-CAM hosts will require a re-wiring of guard cell metabolism.

EXPERIMENTAL PROCEDURES

Plant materials

Kalanchoë fedtschenkoi wild-type (WT) plants were grown in a growth chamber with a 12-h photoperiod, with a photosynthetic photon flux density (PPFD) of 250 $\mu\text{mol m}^{-2} \text{s}^{-1}$ at plant height and with day/night temperatures of 25°C/18°C. Leaf pair 6 (where pair 1 are the youngest leaves growing at the apical zone of the plant) of 12-week-old plants were selected for analysis. The leaf was divided into epidermis tissue and ground mesophyll (i.e. samples 'EP' and 'M', respectively). For sampling purposes, the leaf tip was bent over, which allowed the epidermis to be rapidly and cleanly peeled away from the mesophyll before being snap frozen in liquid N₂. Each biological replicate consisted of epidermal peels taken from the abaxial and adaxial surfaces of leaf pair 6 from one plant. The epidermis and mesophyll were sampled over a 24-h day/night cycle using three biological replicates for each time point (i.e. 08:00 h, dark; 12:00 h, light; 16:00 h, light; 20:00 h, light; 00:00 h, dark; 04:00 h, dark; within the growth chamber, lights came on at 08:30 h and went off at 20:30 h). All samples were immediately snap frozen in liquid nitrogen and stored at -80°C until their evaluation.

Structural characteristics of epidermal peels

The presence and distribution of chloroplasts and mitochondria within cell types present in the epidermal peels was assessed using confocal microscopy and mitochondrial staining. Epidermal peels were incubated in 0.1 M HEPES buffer, pH 7, for 5 min, followed by staining with 10 $\mu\text{g ml}^{-1}$ of Rhodamine 123 (cat. no. R8004; Sigma-Aldrich, <https://www.sigmaaldrich.com>) in the dark at room temperature (20–22°C) for 30 min. Peels were subsequently washed with two changes of 0.1 M HEPES buffer, pH 7, transferred to microscope slides and observed on a LEICA SP8 STED 3X microscope with excitation λ of 511 nm. Chloroplast localization was based on autofluorescence of chlorophyll at an excitation λ of 598 nm.

Malate and starch content

Malate was extracted from leaf mesophyll and epidermal peels as described by Haider *et al.* (2012) and measured using the enzymatic method described by Hohorst (1970).

The starch content of the leaf mesophyll was determined as described by Haider *et al.* (2012). Guard cell starch content was determined by fixing epidermal peels in 50% v/v methanol, 10% v/v acetic acid. Starch granules were stained with a pseudo-schiff propidium iodide and subsequently analyzed using confocal laser scanning microscopy, as described by Flutsch *et al.* (2018).

Gas-exchange analysis

Net CO₂ uptake was determined for leaf number 6 (three biological replicates) over a 24-hr day/night cycle, using the LI-6400XT

Portable Photosynthesis System (LI-COR Environmental, <https://www.licor.com>). Light and temperature within the leaf chamber were set to track the conditions established in the growth chamber, where all measurements were conducted (25°C/19°C and a diurnal PPFD of 250 mol m⁻² s⁻¹ at plant height). The ambient CO₂ concentration was set at 400 μmol CO₂ mol⁻¹ and the relative humidity was maintained between 50 and 60%. Data were recorded every 15 min and plotted against time.

Protein extraction and digestion

Harvested epidermis and mesophyll tissues were suspended in sodium deoxycholate (SDC) lysis buffer (4% in 100 mM of NH₄HCO₃, 10 mM dithiothreitol, DTT). Samples were physically disrupted by bead beating before heating at 90°C for 5 min and then centrifuged to remove cellular debris. Cysteines were blocked by adjusting each sample to 30 mM indole-3-acetic acid (IAA) and incubated in the dark for 15 min at room temperature. Samples were transferred to a 10-kDa molecular weight spin column (Vivaspin 2; GE Healthcare, <https://www.gehealthcare.com>) and filtered. Proteins retained on top of the filter were washed with 100 mM of NH₄HCO₃ and then resuspended in 100 mM of NH₄HCO₃ to adjust samples to 2% SDC. Protein concentrations were estimated by performing a BCA assay (Pierce Biotechnology, now ThermoFisher Scientific, <https://www.thermofisher.com>). Each sample was digested via two aliquots of sequencing-grade trypsin (1:75, w:w; Promega, <https://www.promega.com>) at two different sample dilutions (overnight), and for a subsequent 3 h at 37°C. The peptide mixture was collected by centrifugation and then adjusted to 1% formic acid (FA) to precipitate SDC. Hydrated ethyl acetate was added to each sample at a 1:1 (v:v) ratio three times to effectively remove SDC. Samples were then placed in a SpeedVac Concentrator (ThermoFisher Scientific, <https://www.thermofisher.com>) to remove ethyl acetate and further concentrate the sample. The peptide-enriched flow was quantified by BCA assay, desalted on RP-C18 stage tips (Pierce Biotechnology, now ThermoFisher Scientific) and then stored at -80°C until analysis by liquid chromatography with tandem mass spectrometry (LC-MS/MS).

LC-MS/MS

All samples were analyzed on a Q Exactive Plus mass spectrometer (ThermoFisher Scientific) coupled with a Proxeon EASY-nLC 1200 liquid chromatography pump (ThermoFisher Scientific). Peptides were separated on a 75-μm inner diameter microcapillary column packed with 25 cm of Kinetex C18 resin (1.7 μm, 100 Å; Phenomenex, <https://www.phenomenex.com>). For each sample, a 2-μg aliquot was loaded in buffer A (0.1% FA, 2% acetonitrile) and eluted with a linear 150-min gradient of 2–20% buffer B (0.1% FA, 80% acetonitrile), followed by an increase in buffer B to 30% for 10 min, another increase to 50% buffer B for 10 min and concluding with a 10 min wash with 98% buffer A. The flow rate was kept at 200 nl min⁻¹. MS data were acquired with XCALIBUR™ 4.27.19 (ThermoFisher Scientific), using the top-*N* method where *N* could be up to 15. Target values for the full scan MS spectra were 1 × 10⁶ charges in the 300–1500 *m/z* range, with a maximum injection time of 25 ms. Transient times corresponding to a resolution of 70 000 at *m/z* 200 were chosen. A 1.6 *m/z* isolation window and fragmentation of precursor ions was performed by higher energy C-trap dissociation (HCD), with a normalized collision energy of 30 eV. MS/MS scans were performed at a resolution of 17 500 at *m/z* 200 with an ion target value of 1 × 10⁶ and a maximum injection time of 50 ms. Dynamic exclusion was set to 45 s to avoid the repeated sequencing of peptides.

Peptide identification and protein inference

Raw MS data files were searched against the *K. fedtschenkoii* 1.1 proteome FASTA database appended with the predicted chloroplast and mitochondrial proteins, as well as common contaminants (e.g. trypsin, human keratin, etc.). A decoy database, consisting of the reversed sequences of the target database, was appended to discern the FDR at the spectral level (Elias and Gygi, 2007). For standard database searching, the peptide fragmentation spectra (MS/MS) were analyzed by the CRUX PIPELINE 3.0 (McIlwain *et al.*, 2014). The MS/MS were searched using the Tide algorithm (Diament and Noble, 2011) and configured to derive fully tryptic peptides using default settings except for the following parameters: allowed clip n-term methionine, a precursor mass tolerance of 10 parts per million (ppm), a static modification on cysteines (iodoacetamide; +57.0214 Da) and dynamic modifications on methionine (oxidation; +15.9949). Results were processed by PERCOLATOR (Kall *et al.*, 2007) to estimate the *q* values. Peptide spectrum matches and peptides were considered identified at a *q* value of <0.01. Across the entire experimental data set, proteins were required to have at least two distinct peptide sequences and two minimum spectra per protein. To deal with the redundancy associated with the *K. fedtschenkoii* proteome database, all proteins in the FASTA database were grouped by sequence similarity (≥90%) using the UCLUST component of the USEARCH 5.0 software platform (Edgar, 2010). As described previously (Abraham *et al.*, 2012), grouping proteins by this threshold of sequence identity serves to: (i) maintain biologically relevant peptide information that would have otherwise been lost through protein sequence redundancy; and (ii) eliminate ambiguity in peptide assignments.

Label-free quantification

The MS1-level precursor intensities were derived from modest feature finder (moFF, Argentini *et al.*, 2016) using the following parameters: 10 ppm mass tolerance; a retention time window for extracted ion chromatogram of 3 min; and a time window to get the apex for MS/MS precursor of 30 sec. Protein intensity-based values, which were calculated by summing together quantified peptides, were normalized by dividing by protein length and total ion intensities and then LOESS (locally estimated scatterplot smoothing) and median central tendency procedures were performed on log₂-transformed values by INFERNORDN (Polpitiya *et al.*, 2008).

Statistical analysis for differential abundances

We performed a pair-wise comparison between the collective epidermis (EP08, EP12, EP16, EP20, EP00, EP04) proteome and the collective mesophyll proteome (M08, M12, M16, M20, M00, M04). To improve the robustness of this quantitative analysis, we removed low-abundance and randomly sampled proteins by summing protein intensities across the collective epidermis proteome or mesophyll proteome and calculating a running sum from the most abundant protein to the least abundant protein. The cumulative percentage of each protein in each collective proteome was then used to identify a limit of quantitation (LOQ), which represents the bottom 1%. After filtering the data, a Student's *t*-test was used to identify differences between average protein abundances in each collective proteome. Using PERSEUS (<http://www.perseus-framework.org>) (Tyanova *et al.*, 2016), missing values were replaced by random numbers drawn from a normal distribution (width = 0.3 and downshift = 2.5). A protein was categorized as having a significant abundance

difference between the epidermis peel and mesophyll proteomes if it passed a significance threshold requiring a P value of ≤ 0.05 and absolute value of \log_2 fold-change difference of >1 . Diel changes in protein abundances were tested by an analysis of variance (ANOVA) with *post-hoc* Tukey test and categorized as a significant change in abundance for P values of <0.05 and at least one absolute value of \log_2 fold-change difference of >1 .

Gene ontology enrichment

Whole-genome GO term annotation was performed using BLAST2GO (Conesa *et al.*, 2005) with a blastp E-value hit filter of 1×10^{-5} , an annotation cut-off value of 55 and a GO weight of 5. Using CLUEGO (Bindea *et al.*, 2009), observed GO biological processes were subjected to the right-sided hypergeometric enrichment test at medium network specificity selection and P -value correction was performed using the Holm–Bonferroni step-down method (Holm, 1979). There was a minimum of three and a maximum of eight selected GO tree levels, and each cluster was set to include a minimum of between 3 and 4% of genes associated with each term. Minimal reporting of functional groups was achieved by implementing CLUEGO GO term fusion and grouping settings were selected to reduce GO term redundancy. The term enriched at the highest level of significance was used as the representative term for each functional cluster. The GO terms at adjusted $P \leq 0.05$ were considered significantly enriched.

ACKNOWLEDGEMENTS

This material is based upon work supported by the Department of Energy Office of Science Genomic Science Program under award number DE-SC0008834. This research used resources of the Compute and Data Environment for Science (CADES) at the Oak Ridge National Laboratory. Oak Ridge National Laboratory is managed by UT-Battelle, LLC for the US Department of Energy (under contract number DE-AC05-00OR22725). Additional funding was provided by Colciencias (NHC), BBSRC (DCT) and the Swiss National Science Foundation (SF) (grant no. 31003A-166539/1 to DS).

This manuscript has been authored by UT-Battelle, LLC under contract no. DE-AC05-00OR22725 with the US Department of Energy. The publisher, by accepting the article for publication, acknowledges that the United States Government retains a non-exclusive, paid-up, irrevocable, world-wide license to publish or reproduce the published form of this manuscript, or allow others to do so, for United States Government purposes. The Department of Energy will provide public access to these results of federally sponsored research in accordance with the DOE Public Access Plan (<http://energy.gov/downloads/doe-public-access-plan>)

AUTHOR CONTRIBUTIONS

AMB, PEA, NHC and JB contributed to the conception and design of the experiments, PEA, NHC and SF contributed to the acquisition of data, PEA, NHC, AMB, DCY, SP, SF and DS contributed to data analysis and interpretation, AMB and PEA drafted the manuscript, and all authors critically revised and approved the final version of the manuscript for publication.

CONFLICT OF INTEREST

The authors declare no financial conflicts of interest.

DATA AVAILABILITY STATEMENT

The protein data and all supplementary tables have been deposited at ProteomeXchange (Vizcaino *et al.*, 2014) and the accession is PXD010837.

SUPPORTING INFORMATION

Additional Supporting Information may be found in the online version of this article.

Figure S1. (a) The distribution of cumulative protein intensities (i.e. running sum) across the entire epidermal peel and mesophyll illustrates the relative contribution of each protein from the most abundant to least abundant protein. (b) The distribution of cumulative protein intensities (i.e. running sum) across the entire epidermal peel and mesophyll after removing the bottom 1% of quantitative information for both the epidermal peel and mesophyll total proteomes. The inset bar graph highlights the number of proteins available for differential analyses following this operation (yellow bar). (c) Two-way hierarchical cluster (Fast Ward) of \log_2 normalized protein abundances for the unfiltered data and (d) filtered data in which the bottom 1% was removed.

Figure S2. (a) The distribution of median protein abundances across mesophyll or epidermal data was illustrated by a violin plot. The deciles are marked for each plot. A functional enrichment test for the most abundant proteins (10th decile; green) found in the mesophyll or epidermal layers highlights investments into two major GO functional processes. (b) The 10% most abundant proteins cover more enriched GO terms with highest coverage in plant defense and cell fate signaling pathways for epidermal peels and photosynthesis and carbohydrate metabolism in mesophyll.

Figure S3. Volcano plot for pairwise comparison between the epidermal (upper peel only) and mesophyll data sets. Proteins that passed the required thresholds for significance are plotted. The proteins that were exclusively identified in the epidermal (red) and mesophyll (blue) are highlighted.

Figure S4. Proteins that passed the ANOVA test were evaluated using the gap statistic method for k -means to identify the optimal number of clusters for the (a) epidermal peel data set (red; dotted line $n = 10$) and (b) mesophyll data set (blue; dotted line $n = 14$). The number of proteins and % of total proteins from ANOVA tests is reported for each (c) epidermal peel cluster and (d) mesophyll cluster.

Figure S5. C_4 metabolism. The relative abundance of each protein across the diel cycle is shown for the epidermal (red) and mesophyll data sets as a line plot. ‘***’ represents proteins that passed the significance threshold from the ANOVA test. For each box plot, the average abundance of a protein in the epidermal and mesophyll data set is represented and ‘*’ represents proteins that passed the maximum versus minimum Student’s t -test threshold.

Figure S6. Glycolysis/gluconeogenesis. The relative abundance of each protein across the diel cycle is shown for the epidermal (red) and mesophyll data sets as a line plot. ‘***’ represents proteins that passed the significance threshold from the ANOVA test. For each box plot, the average abundance of a protein in the epidermal and mesophyll data set is represented and ‘*’ represents proteins that passed the maximum versus minimum Student’s t -test threshold.

Figure S7. Starch metabolism. The relative abundance of each protein across the diel cycle is shown for the epidermal (red) and

mesophyll data sets as a line plot. ‘***’ represents proteins that passed the significance threshold from the ANOVA test. For each box plot, the average abundance of a protein in the epidermal and mesophyll data set is represented and ‘**’ represents proteins that passed the maximum versus minimum Student’s *t*-test threshold.

Table S1. Verbose listing of peptides identified with $q < 0.01$ that map to proteins having at least two distinct peptides. The quantitative value (i.e. moFF intensity) is provided per peptide per sample.

Table S2. Verbose listing of proteins identified. The quantitative value (i.e. normalized moFF intensity) is provided per protein per sample.

Table S3. Data matrix of proteins that passed the limit of quantification (LOQ). The quantitative value (i.e. moFF intensity) is provided per protein per sample. Null values were replaced with an imputed value drawn from a random distribution using PERSEUS (width = 0.3, downshift = 2.5).

Table S4. Student’s *t*-test results for epidermal peel versus mesophyll.

Table S5. Gene ontology enrichment results (CLUEGO) for epidermal peel-enriched protein abundances.

Table S6. Gene ontology enrichment results (CLUEGO) for mesophyll-enriched protein abundances.

Table S7. Epidermal peel proteins that have significant variation in relative abundance across the measured diel period. For each protein, the *k*-mean cluster is provided.

Table S8. Mesophyll proteins that have significant variation in relative abundance across the measured diel period. For each protein, the *k*-mean cluster is provided.

Table S9. Frequency of gene ontology (GO) phrases using controlled vocabularies for epidermal peel proteins that have significant variation in relative abundance across the measured diel period. For each protein, the *k*-mean cluster is provided.

Table S10. Frequency of gene ontology (GO) phrases using controlled vocabularies for mesophyll proteins that have significant variation in relative abundance across the measured diel period. For each protein, the *k*-mean cluster is provided.

Table S11. Database search results when considering the dynamic phosphorylation modification (1STY+79.966331). Verbose listing of peptides identified with $q < 0.01$ that map to proteins having at least two distinct peptides. The quantitative value (i.e. moFF intensity) is provided per peptide per sample.

REFERENCES

- Abraham, P., Adams, R., Giannone, R.J., Kalluri, U., Ranjan, P., Erickson, B., Shah, M., Tuskan, G.A. and Hettich, R.L. (2012) Defining the boundaries and characterizing the landscape of functional genome expression in vascular tissues of *Populus* using shotgun proteomics. *J. Proteome Res.* **11**, 449–60.
- Abraham, P.E., Yin, H.F., Borland, A.M. et al. (2016) Transcript, protein and metabolite temporal dynamics in the CAM plant *Agave*. *Nat. Plants*, **2**, Artn 16178.
- Akoh, C.C., Lee, G.C., Liaw, Y.C., Huang, T.H. and Shaw, J.F. (2004) GDSL family of serine esterases/lipases. *Prog. Lipid Res.* **43**, 534–552.
- Araujo, W.L., Nunes-Nesi, A. and Fernie, A.R. (2014) On the role of plant mitochondrial metabolism and its impact on photosynthesis in both optimal and sub-optimal growth conditions. *Photosynth. Res.* **119**, 141–156.
- Argentini, A., Goeminne, L.J.E., Verheggen, K., Hulstaert, N., Staes, A., Clement, L. and Martens, L. (2016) moFF: a robust and automated approach to extract peptide ion intensities. *Nat. Methods*, **13**, 962–965.
- Azoulay-Shemer, T., Bagheri, A., Wang, C., Palomares, A., Stephan, A.B., Kunz, H.H. and Schroeder, J.I. (2016) Starch biosynthesis in guard cells but not in mesophyll cells is involved in CO₂-induced stomatal closing. *Plant Physiol.* **171**, 788–798.
- Balsamo, R.A. and Uribe, E.G. (1988) Leaf anatomy and ultrastructure of the crassulacean-acid-metabolism plant *Kalanchoe daigremontiana*. *Planta*, **173**, 183–189.
- Berardini, T.Z., Mundodi, S., Reiser, L. et al. (2004) Functional annotation of the Arabidopsis genome using controlled vocabularies. *Plant Physiol.* **135**, 745–755.
- Bernard, A. and Joubes, J. (2013) Arabidopsis cuticular waxes: advances in synthesis, export and regulation. *Prog. Lipid Res.* **52**, 110–129.
- Bindea, G., Mlecnik, B., Hackl, H., Charoentong, P., Tosolini, M., Kirilovsky, A., Fridman, W.H., Pages, F., Trajanoski, Z. and Galon, J. (2009) ClueGO: a Cytoscape plug-in to decipher functionally grouped gene ontology and pathway annotation networks. *Bioinformatics*, **25**, 1091–1093.
- Borland, A.M., Griffiths, H., Hartwell, J. and Smith, J.A. (2009) Exploiting the potential of plants with crassulacean acid metabolism for bioenergy production on marginal lands. *J. Exp. Bot.* **60**, 2879–2896.
- Borland, A.M., Hartwell, J., Weston, D.J., Schlauch, K.A., Tschaplinski, T.J., Tuskan, G.A., Yang, X. and Cushman, J.C. (2014) Engineering crassulacean acid metabolism to improve water-use efficiency. *Trends Plant Sci.* **19**, 327–338.
- Borland, A.M., Wullschlegel, S.D., Weston, D.J., Hartwell, J., Tuskan, G.A., Yang, X. and Cushman, J.C. (2015) Climate-resilient agroforestry: physiological responses to climate change and engineering of crassulacean acid metabolism (CAM) as a mitigation strategy. *Plant Cell Environ.* **38**, 1833–1849.
- Borland, A.M., Guo, H.B., Yang, X.H. and Cushman, J.C. (2016) Orchestration of carbohydrate processing for crassulacean acid metabolism. *Curr. Opin. Plant Biol.* **31**, 118–124.
- Borland, A.M., Leverett, A., Hurtado-Castano, N., Hu, R. and Yang, X. (2018) Functional anatomical traits of the photosynthetic organs of plants with crassulacean acid metabolism. In *The Leaf: A Platform for Performing Photosynthesis* (Adams III W.W. and Terashima, I., eds). Cham: Springer International Publishing.
- Bouche, N. and Fromm, H. (2004) GABA in plants: just a metabolite? *Trends Plant Sci.* **9**, 110–115.
- Boxall, S.F., Dever, L.V., Knerova, J., Gould, P.D. and Hartwell, J. (2017) Phosphorylation of phosphoenolpyruvate carboxylase is essential for maximal and sustained dark CO₂ fixation and core circadian clock operation in the obligate crassulacean acid metabolism species *Kalanchoe fedtschenkoi*. *Plant Cell*, **29**, 2519–2536.
- Boxall, S.F., Kardu, N., Dever, L.V., Knerova, J., Waller, J.L., Gould, P.D. and Hartwell, J. (2020) *Kalanchoe* PPC1 is essential for crassulacean acid metabolism and the regulation of core circadian clock and guard cell signalling genes. *Plant Cell*, <https://doi.org/10.1105/tpc.19.00481>
- Ceusters, N., Frans, M., van den Ende, W. and Ceusters, J. (2019) Maltose processing and not β -amylase activity curtails hydrolytic starch degradation in the CAM orchid *Phalaenopsis*. *Front Plant Sci.* **10**, 1386.
- Chastain, C.J., Lee, M.E., Moorman, M.A., Shameekumar, P. and Chollet, R. (1997) Site-directed mutagenesis of maize recombinant C-4-pyruvate, orthophosphate dikinase at the phosphorylatable target threonine residue. *FEBS Lett.* **413**, 169–173.
- Conesa, A., Gotz, S., Garcia-Gomez, J.M., Terol, J., Talon, M. and Robles, M. (2005) Blast2GO: a universal tool for annotation, visualization and analysis in functional genomics research. *Bioinformatics*, **21**, 3674–3676.
- Costa, S.S., Muzitano, M.F., Camargo, L.M.M. and Coutinho, M.A.S. (2008) Therapeutic potential of *Kalanchoe* species: flavonoids and other secondary metabolites. *Natural Product Commun.* **3**, 2151–2164.
- Depaoli, H.C., Borland, A.M., Tuskan, G.A., Cushman, J.C. and Yang, X. (2014) Synthetic biology as it relates to CAM photosynthesis: challenges and opportunities. *J. Exp. Bot.* **65**, 3381–3393.
- Dever, L.V., Boxall, S.F., Knerova, J. and Hartwell, J. (2015) Transgenic perturbation of the decarboxylation phase of Crassulacean acid metabolism alters physiology and metabolism but has only a small effect on growth. *Plant Physiol.* **167**, 44–59.
- Diament, B.J. and Noble, W.S. (2011) Faster SEQUEST searching for peptide identification from tandem mass spectra. *J. Proteome Res.* **10**, 3871–3879.
- Edgar, R.C. (2010) Search and clustering orders of magnitude faster than BLAST. *Bioinformatics*, **26**, 2460–2461.

- Elias, J.E. and Gygi, S.P. (2007) Target-decoy search strategy for increased confidence in large-scale protein identifications by mass spectrometry. *Nat. Methods*, **4**, 207–214.
- Fernie, A.R. and Martinioia, E. (2009) Malate. Jack of all trades or master of a few? *Phytochemistry*, **70**, 828–832.
- Flutsch, S., Distefano, L. and Santelia, D. (2018) Quantification of starch in guard cells of *Arabidopsis thaliana*. *Bio-protocol*, **8**, e2920. <https://doi.org/10.21769/BioProtoc.2920>.
- Fricker, M. and Willmer, C. (1996) *Stomata*. The Netherlands: Springer.
- Geiger, D., Scherzer, S., Mumm, P. et al. (2010) Guard cell anion channel SLAC1 is regulated by CDPK protein kinases with distinct Ca²⁺ affinities. *Proc. Natl Acad. Sci. USA*, **107**, 8023–8028.
- Gronin, A., Rodrigues, O., Verdoucq, L., Merlot, S., Leonhardt, N. and Maurel, C. (2015) Aquaporins contribute to ABA-triggered stomatal closure through OST1-mediated phosphorylation. *Plant Cell*, **27**, 1945–1954.
- Groszmann, M., Osborn, H.L. and Evans, J.R. (2017) Carbon dioxide and water transport through plant aquaporins. *Plant Cell Environ.* **40**, 938–961.
- Hahlbrock, K. and Scheel, D. (1989) Physiology and molecular-biology of phenylpropanoid metabolism. *Annu. Rev. Plant Physiol. Plant Mol. Biol.* **40**, 347–369.
- Haider, M.S., Barnes, J.D., Cushman, J.C. and Borland, A.M. (2012) A CAM- and starch-deficient mutant of the facultative CAM species *Mesembryanthemum crystallinum* reconciles sink demands by repartitioning carbon during acclimation to salinity. *J. Exp. Bot.* **63**, 1985–1996.
- Hartwell, J., Dever, L.V. and Boxall, S.F. (2016) Emerging model systems for functional genomics analysis of Crassulacean acid metabolism. *Curr. Opin. Plant Biol.* **31**, 100–108.
- Heinen, R.B., Ye, Q. and Chaumont, F. (2009) Role of aquaporins in leaf physiology. *J. Exp. Bot.* **60**, 2971–2985.
- Hohorst, H.J. (1970) L-malate estimation with malate dehydrogenase and NAD. In *Methods in Enzymatic Analysis* (Bergmeyer, H.V., ed). Weinheim, Germany: Verlag Chemie.
- Holm, S. (1979) A simple sequentially rejective multiple test procedure. *Scand. J. Stat.* **6**, 65–70.
- Holtum, J.A.M., Smith, J.A.C. and Neuhaus, H.E. (2005) Intracellular transport and pathways of carbon flow in plants with crassulacean acid metabolism. *Funct. Plant Biol.* **32**, 429–449.
- Horrer, D., Flutsch, S., Pazmino, D., Matthews, J.S., Thalmann, M., Nigro, A., Leonhardt, N., Lawson, T. and Santelia, D. (2016) Blue light induces a distinct starch degradation pathway in guard cells for stomatal opening. *Curr. Biol.* **26**, 362–370.
- Hu, H., Boisson-Dernier, A., Israelsson-Nordstrom, M., Bohmer, M., Xue, S., Ries, A., Godoski, J., Kuhn, J.M. and Schroeder, J.I. (2010) Carbonic anhydrases are upstream regulators of CO₂-controlled stomatal movements in guard cells. *Nat. Cell Biol.* **12**, 87–93; sup pp 1–18.
- Hu, H., Rappell, W.J., Occhipinti, R., Ries, A., Bohmer, M., You, L., Xiao, C., Engineer, C.B., Boron, W.F. and Schoeder, J.I. (2015) Distinct cellular localization of carbonic anhydrases mediate carbon dioxide control of stomatal movements. *Plant Physiol.* **169**, 1168–1178.
- Kall, L., Canterbury, J.D., Weston, J., Noble, W.S. and Maccoss, M.J. (2007) Semi-supervised learning for peptide identification from shotgun proteomics datasets. *Nat. Methods*, **4**, 923–925.
- Kim, J.M., To, T.K., Matsui, A. et al. (2017) Acetate-mediated novel survival strategy against drought in plants. *Nat. Plants*, **3**, 17097.
- Lai, L.B., Wang, L. and Nelson, T.M. (2002) Distinct but conserved functions for two chloroplastic NADP-malic enzyme isoforms in C-3 and C-4 Flaveria species. *Plant Physiol.* **128**, 125–139.
- Lamesch, P., Berardini, T.Z., Li, D.H. et al. (2012) The Arabidopsis Information Resource (TAIR): improved gene annotation and new tools. *Nucleic Acids Res.* **40**, D1202–D1210.
- Laporte, M.M., Shen, B. and Tarczynski, M.C. (2002) Engineering for drought avoidance: expression of maize NADP-malic enzyme in tobacco results in altered stomatal function. *J. Exp. Bot.* **53**, 699–705.
- Males, J. and Griffiths, H. (2017) Stomatal biology of CAM plants. *Plant Physiol.* **174**, 550–560.
- Malinova, I. and Fettke, J. (2017) Reduced starch granule number per chloroplast in the dpe2/phs1 mutant is dependent on initiation of starch degradation. *PLoS ONE*, **12**, e0187985.
- Martinioia, E. and Rentsch, D. (1994) Malate compartmentation - responses to a complex metabolism. *Annu. Rev. Plant Physiol. Plant Mol. Biol.* **45**, 447–467.
- Maurino, V.G., Drincovich, M.F., Casati, P., Andreo, C.S., Edwards, G.E., Ku, M.S.B., Gupta, S.K. and Franceschi, V.R. (1997) NADP-malic enzyme: immunolocalization in different tissues34 plant maize and the C3 plant wheat. *J. Exp. Bot.* **48**, 799–811.
- McIlwain, S., Tamura, K., Kertesz-Farkas, A. et al. (2014) Crux: rapid open source protein tandem mass spectrometry analysis. *J. Proteome Res.* **13**, 4488–4491.
- Mintz-Oron, S., Mandel, T., Rogachev, I. et al. (2008) Gene expression and metabolism in tomato fruit surface tissues. *Plant Physiol.* **147**, 823–851.
- Monroe, J.D. and Storm, A.R. (2018) Review: The Arabidopsis beta-amylase (BAM) gene family: diversity of form and function. *Plant Sci.* **276**, 163–170.
- Monroe, J.D., Pope, L.E., Breault, J.S., Berndsen, C.E. and Storm, A.R. (2018) Quaternary structure, salt sensitivity, and allosteric regulation of beta-AMYLASE2 from *Arabidopsis thaliana*. *Front. Plant Sci.* **9**, 1176.
- Mount, D.W. (2007) Using the basic local alignment search tool (BLAST). *CSH Protoc.* **2007**, pdb top17.
- Oparka, K.J. and Roberts, A.G. (2001) Plasmodesmata. A not so open-and-shut case. *Plant Physiol.* **125**, 123–126.
- Outlaw, W.H., Manchester, J. and Brown, P.H. (1981) High levels of malic enzyme activities in *Vicia faba* L. epidermal tissue. *Plant Physiol.* **68**, 1047–1051.
- Polpitiya, A.D., Qian, W.J., Jaitly, N., Petyuk, V.A., Adkins, J.N., Camp, D.G. 2nd, Anderson, G.A. and Smith, R.D. (2008) DAnTE: a statistical tool for quantitative analysis of -omics data. *Bioinformatics*, **24**, 1556–1568.
- Rodrigues, M.A., Matiz, A., Cruz, A.B. et al. (2013) Spatial patterns of photosynthesis in thin- and thick-leaved epiphytic orchids: unravelling C3-CAM plasticity in an organ-compartmented way. *Ann. Bot.* **112**, 17–29.
- Santelia, D. and Lawson, T. (2016) Rethinking guard cell metabolism. *Plant Physiol.* **172**, 1371–1392.
- Schnabl, H. (1980) CO₂ and malate metabolism in starch-containing and starch-lacking guard-cell protoplasts. *Planta*, **149**, 52–58.
- Shameer, S., Baghalian, K., Cheung, C.Y.M., Ratcliffe, R.G. and Sweetlove, L.J. (2018) Computational analysis of the productivity potential of CAM. *Nat. Plants*, **4**, 165–171.
- Shepherd, T. and Griffiths, D.W. (2006) The effects of heat stress on plant cuticular waxes. *New Phytol.* **171**, 469–499.
- Suh, M.C., Samuels, A.L., Jetter, R., Kunst, L., Pollard, M., Ohrogge, J. and Beisson, F. (2005) Cuticular lipid composition, surface structure, and gene expression in Arabidopsis stem epidermis. *Plant Physiol.* **139**, 1649–1665.
- Tibshirani, R., Walther, G. and Hastie, T. (2001) Estimating the number of clusters in a data set via the gap statistic. *J. R. Statist. Soc. Series B-Statist. Methodol.* **63**, 411–423.
- Tyanova, S., Temu, T., Sinitcyn, P., Carlson, A., Hein, M.Y., Geiger, T., Mann, M. and Cox, J. (2016) The Perseus computational platform for comprehensive analysis of (prote)omics data. *Nat. Methods*, **13**, 731–740.
- Ueno, K., Kinoshita, T., Inoue, S., Emi, T. and Shimazaki, K. (2005) Biochemical characterization of plasma membrane H⁺-ATPase activation in guard cell protoplasts of *Arabidopsis thaliana* in response to blue light. *Plant Cell Physiol.* **46**, 955–963.
- Vizcaino, J.A., Deutsch, E.W., Wang, R. et al. (2014) ProteomeXchange provides globally coordinated proteomics data submission and dissemination. *Nat. Biotechnol.* **32**, 223–226.
- Wang, X.-C., Outlaw, W.H., De Bedout, J.A. and Du, Z. (1994) Kinetic characterisation of phosphoenolpyruvate carboxylase extraction from whole leaf and from guard cell protoplasts of *Vicia faba* L. (C3 plant) with respect to tissue pre-illumination. *Histochem. J.* **26**, 152–160.
- Wheeler, M.C.G., Tronconi, M.A., Drincovich, M.F., Andreo, C.S., Flugge, U.I. and Maurino, V.G. (2005) A comprehensive analysis of the NADP-malic enzyme gene family of Arabidopsis. *Plant Physiol.* **139**, 39–51.
- Willmer, C.M. and Pallas, J.E. (1973) Survey of stomatal movements and associated potassium fluxes in plant kingdom. *Canadian J Bot-Revue Canadienne De Botan.* **51**, 37.
- Xu, M.Z., Chen, F., Qi, S.L., Zhang, L.S. and Wu, S. (2018) Loss or duplication of key regulatory genes coincides with environmental adaptation of the stomatal complex in *Nymphaea colorata* and *Kalanchoe laxiflora*. *Hortic. Res.* **5** <https://doi.org/10.1038/s41438-018-0048-8>

Yang, X., Cushman, J.C., Borland, A.M. et al. (2015) A roadmap for research on crassulacean acid metabolism (CAM) to enhance sustainable food and bioenergy production in a hotter, drier world. *New Phytol.* **207**, 491–504.

Yang, X., Hu, R., Yin, H. et al. (2017) The Kalanchoe genome provides insights into convergent evolution and building blocks of crassulacean acid metabolism. *Nat. Commun.* **8**, 1899.

Yao, X., Xiong, W., Ye, T. and Wu, Y. (2012) Overexpression of the aspartic protease ASPG1 gene confers drought avoidance in Arabidopsis. *J. Exp. Bot.* **63**, 2579–2593.

Zhang, J.B., De-Oliveira-ceciliato, P., Takahashi, Y. et al. (2018) Insights into the molecular mechanisms of CO₂-mediated regulation of stomatal movements. *Curr. Biol.* **28**, R1356–R1363.